Chapter 4

Absorption spectroscopy of atmospheric trace gases

UV-vis absorption spectroscopy using extraterrestrial light sources is a widely used technique for the measurement of atmospheric trace gases, in particular for remote sensing of stratospheric species. For the satellite measurements presented here solar radiation scattered from the atmosphere or reflected from the ground serves as a light source. Some of the characteristics of the sun as light source are discussed in section 4.1. The following sections deal with the principles of absorption spectroscopy and the details of differential optical absorption spectroscopy (DOAS) applied to the satellite data.

4.1 Solar radiation

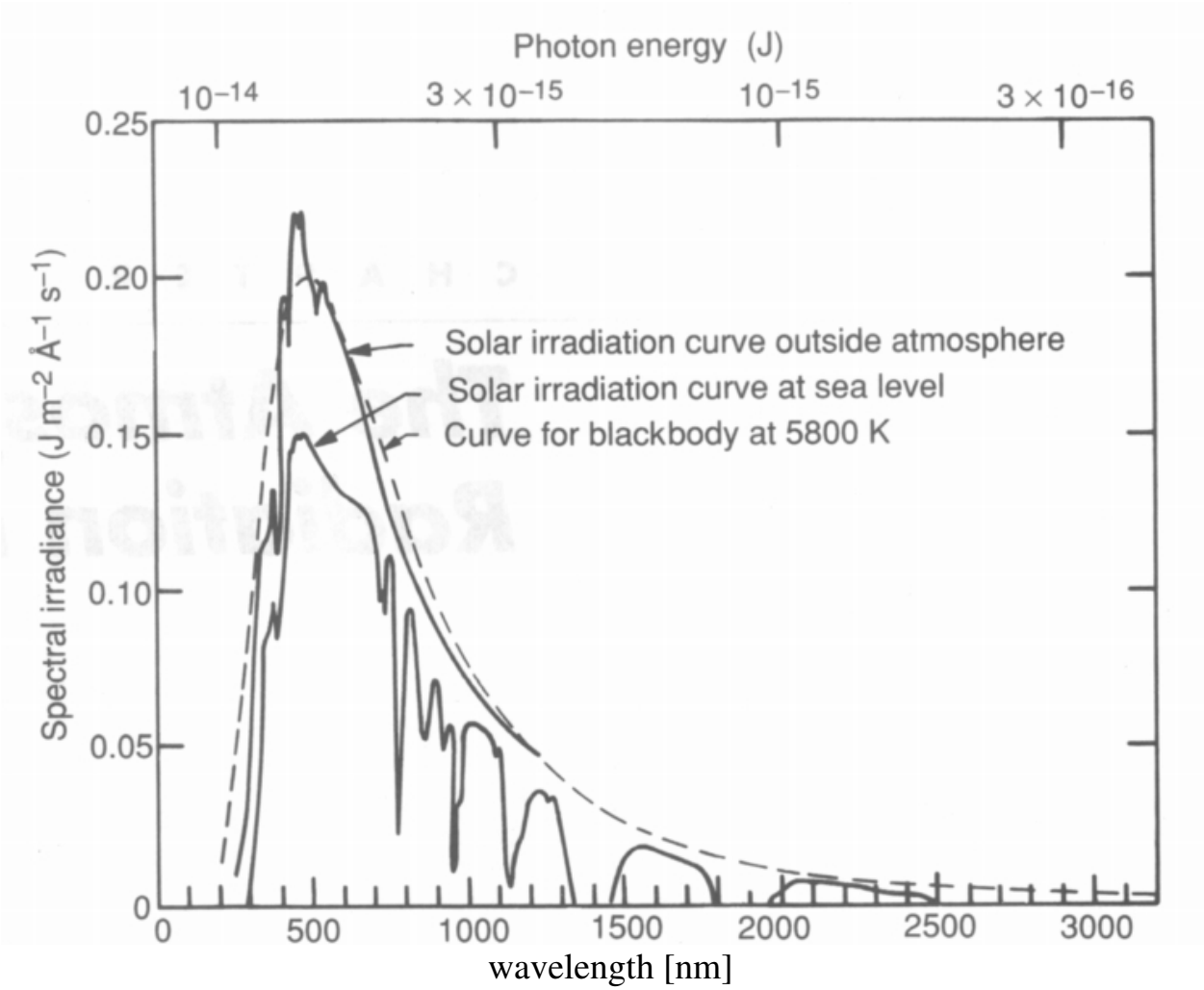

Figure 4.1 The spectrum of solar radiation outside the Earth's atmosphere and at sea level (solid lines) compared with black body radiation at 5800 K (dashed line). The atmospheric absorptions are mainly due to O_3, O_2, H_2O and CO_2 [Graedel and Crutzen, 1993].

The nature of the radiation emitted by the sun is determined by the physical and chemical composition of the sun and especially its atmosphere. The energy originates from a chain of nuclear reactions converting H into He; the temperature of the sun's interior is believed to be $2 \cdot 10^7$ K. The energy is radiated to the upper convective levels, undergoing a series of absorption and emission processes. Most of the solar radiation reaching the earth's atmosphere originates from the so called photosphere, a relatively thin layer (about 1000 km) at the sun's surface. This layer defines the visible area of the sun, its effective temperature is about 5800 K [Brusa and Frohlich, 1982]. The spectrum of the photosphere is a continuum (matching the black body spectrum of about 5800 K, see Figure 4.1) with relatively strong absorption lines called the Fraunhofer lines (named after the physicist Josef Fraunhofer, 1787 - 1826) who discovered dark lines in the solar spectrum (Figure 4.2).
Most of these lines are the result of selective absorption and re-emission of radiation in the upper solar photosphere. Compared to the absorptions of most absorbers of the terrestrial atmosphere the solar Fraunhofer lines are substantially stronger. In particular in the UV-vis range (above 300 nm) they are the dominant features in spectra taken by the GOME instrument (and also by ground based instruments) (see Figure 4.2.).

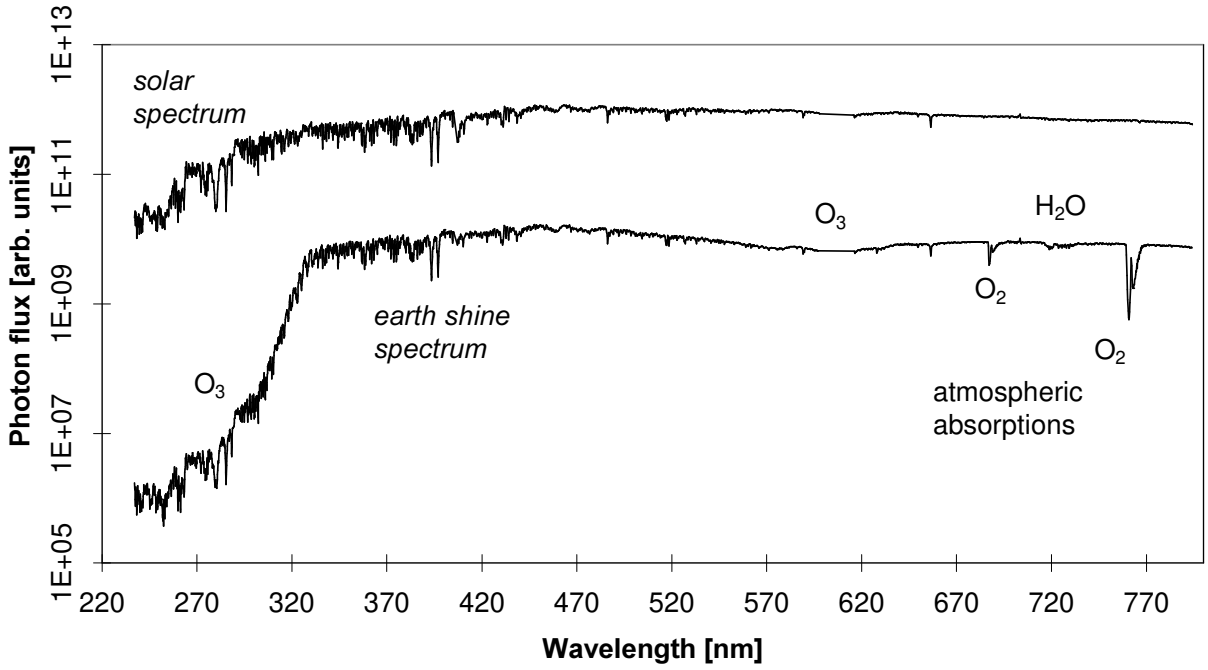

Figure 4.2. GOME spectra (photon fluxes) of the direct sun light and the light reflected from the earth. Both spectra show large structures (Fraunhofer lines) which are caused by absorptions in the solar atmosphere (especially below about 450 nm). In the earth shine spectrum also some prominent atmospheric absorptions of O_2, H_2O and O_3 can bee seen. It should be noted that the absorptions of many atmospheric species (i.e. BrO and OClO) are about two orders of magnitude smaller.

The radiation varies with time due to several phenomena. Observations indicate a fairly regular variation in the occurrence of sun spots with a period of about 11 years, the so called solar cycle.

Sun spots are relatively dark regions in the photosphere with temperatures of about 3000 K and are usually grouped at so called active regions [Brasseur and Solomon, 1984]. In the presence of sun spots the solar irradiation is increased. Besides the 11-year solar cycle this leads also to a 28 day variation due to the sun's rotation [Weber et al., 1998]. Analysis of observed data suggests that the variability in solar irradiance during the 11 year solar cycle depends strongly on the wavelength region. Between 140 to 150 nm it is of the order of 100 %, at 170 nm about 70% and about 20 % at 180 nm. Beyond 300 nm it becomes less than 1 % [Brasseur and Solomon, 1984].

4.2 Interaction of radiation and matter in the UV/vis spectral region

The absorption and emission of energy by molecules is accompanied by a change in the internal energy of the molecule. Photons of the UV/vis wavelength region have energies in the range of about several electron volts. This radiation is high enough to cause electronic transitions when it is absorbed. These electronic transitions are usually accompanied by changes in the vibrational and rotational state of the molecule. Pure vibrational and rotational transitions correspond to lower energies of the infrared and microwave region, respectively. Due to the specific properties of a given molecule its absorption spectrum (or emission spectrum) in the UV/vis spectral range is a characteristic combination of electronic, vibrational and rotational transitions. This is the basis for the selective analysis by spectroscopic techniques.
In the absence of molecular collisions and motion, the natural width of a spectral line is very narrow and depends on the radiative lifetime of the excited state. For atmospheric conditions the natural width is by far smaller compared to Doppler and pressure broadening, which are caused by thermal motion and the collisions between the molecules.
In the atmosphere, pressure broadening is important at low altitudes (a Lorentz line shape is generally assumed):

$$\sigma_{\bar{\nu}} = \frac{S \cdot \gamma_L}{\pi\left((\bar{\nu} - \bar{\nu}_0)^2 + \gamma_{L^2}\right)} \tag{4.1}$$

Here $\bar{\sigma}_0$ represents the absorption cross section and $\bar{\nu}$ the wavenumber. $\bar{\nu}_0$ is the midpoint on the line, S the integrated intensity of the line and γ_L indicates the Lorentz half width of the line. Since the molecular collision frequency varies with pressure and temperature, γ_L can be written as:

$$\gamma_L = \gamma_{L,0} \frac{p}{p_0} \left(\frac{T_0}{T} \right)^{0.5} \tag{4.2}$$

Here $\gamma_{L,0}$ represents the width of the line at standard pressure (p_0 = 1013 hPa) and standard temperature (T_0 = 273 K), typically 0.1 cm^{-1}.

In the upper stratosphere, Doppler broadening becomes equal or even larger than pressure broadening. The absorption cross section for a purely Doppler broadened line is given by:

$$\sigma_{\bar{\nu}} = \frac{S}{\gamma_D \sqrt{\pi}} \exp\left(\frac{-(\bar{\nu} - \bar{\nu}_0)^2}{{\gamma_D}^2} \right) \tag{4.3}$$

Here γ_D denotes the Doppler half-width; for a Maxwell distribution it is:

$$\gamma_D = \frac{\bar{\nu}_0}{c} \sqrt{\frac{8 \cdot \ln 2 \cdot k \cdot T}{m}} \tag{4.4}$$

where *k* is the Boltzmann constant, c the velocity of light and T the temperature.
In the transition region between the Lorentz and the Doppler regimes, the line shape is determined by both broadening processes. If they can be assumed to be independent, they may be combined and a Voigt line profile can be used to describe the absorption line profile.

$$\sigma_{\bar{\nu}} = \frac{a \cdot S}{\gamma_D \cdot \pi^{1.5}} \int_{-\infty}^{\infty} \frac{\exp(-y)^2}{a^2 + (v - y)^2} dy \tag{4.5}$$

with

$$a = \frac{\gamma_L}{\gamma_D}, \qquad v = \frac{(\bar{\nu} - \bar{\nu}_0)}{\gamma_D}, \qquad y = \frac{u}{u_m} \tag{4.6}$$

Here u is the velocity of the molecules in the direction of the observer and u_m is the most probable speed of the molecule [Brasseur and Solomon, 1984; Fish, 1994].
The Voigt line shape resembles the Doppler line shape near the centre and the Lorentz line shape in the wings of the absorption.

While in the microwave and infrared region it is often possible to resolve the individual lines, in the UV/vis spectral range the typical resolution of the instruments usually does not allow to resolve individual lines. For example the full width at half maximum of the GOME instrument in the UV range is about 0.2 nm, much larger than the atmospheric widths of the absorbing molecules. However, in particular for the modelling of the measurements of strong atmospheric absorbers like O_2 and H_2O Doppler and pressure broadening have to be considered, in particular for if there is an overlap of lines [Bösch, 1998].

4.2.1 The Beer-Lambert Law

The absorption of radiation by matter is described by the Beer-Lambert law. The absorption of light of the intensity $I(\lambda)$ at the wavelength λ as it passes through an infinitesimally thin layer of an absorbing matter ds is:

$$dI(\lambda) = I(\lambda) \cdot \rho(s) \cdot \sigma(\lambda, T) ds \tag{4.7}$$

Here $\sigma(\lambda,T)$ is the absorption cross section of the absorbing species which depends on the wavelength and temperature and $\rho(s)$ is its concentration. Integration of equation 4.7 for a finite light path through the absorbing species leads to the relationship between the incident light intensity $I_0(\lambda)$ and the transmitted light intensity $I(\lambda)$, known as the Beer-Lambert law:

$$I(\lambda, \sigma) = I_0(\lambda) \exp\left(-\sigma(\lambda, T) \int \rho(s) ds\right) \tag{4.8}$$

The logarithm of the ratio of the measured I and I_0 is called optical density $\tau(\lambda)$.

$$\tau := -\ln\left(\frac{I(\lambda, \sigma)}{I_0(\lambda)}\right) = \sigma(\lambda, T) \int \rho(s) ds =: \sigma(\lambda, T) \cdot SCD \tag{4.9}$$

From $\tau(\lambda)$ the (slant) column density[1] $\text{SCD} := \int \rho(s)\, ds$ of the absorbing species can be calculated; if the concentration is constant along the absorption path the concentration can be derived.

4.3 Differential optical absorption spectroscopy (DOAS)

The Beer-Lambert law can not directly be applied to atmospheric measurements because of several reasons:
a) Besides the absorption of the trace gases also light extinction occurs due to scattering on molecules and aerosols. Especially for aerosols this extinction can not be corrected for with the desired accuracy.
b) In the atmosphere the absorptions of several species always add up to the total absorption. Thus in most of the cases it is not possible to measure one specific species.
c) In the case of satellite measurements the detected intensity can strongly depend on the ground albedo.

[1] For atmospheric absorption measurements using extraterrestrial light sources the measured column density refers to the integrated trace gas concentration along the 'slant' light path. It is thus usually called slant column density, SCD.

These restrictions can be avoided by applying the method of differential optical absorption spectroscopy (DOAS).

The DOAS technique relies on the measurement of absorption spectra instead of monochromatic light (Equation 4.8). Thus it is possible to separate the absorption structures of several atmospheric species from each other as well as from the extinction due to scattering on molecules and aerosols. The DOAS method was introduced by Perner and Platt [1979], a detailed description can be found in Platt [1994].
The key principle of DOAS is the separation of the absorption in a part which represents broad spectral features and in a part representing narrow spectral features. Consequently $\sigma(\lambda)$ of a certain absorbing species is split into a portion $\sigma_c(\lambda)$ which varies only 'slowly' with the wavelength λ and into a portion $\sigma'(\lambda)$ which shows 'rapid' variation with λ:

$$\sigma(\lambda) = \sigma_c(\lambda) + \sigma'(\lambda). \tag{4.10}$$

The definition of the threshold between 'slow' and 'rapid' variation of the absorption cross-section as a function of wavelength depends on the observed wavelength interval and the width of the absorption bands to be detected. Commonly the spectra are filtered by dividing by a fitted polynomial or by a smoothed spectrum. Conventionally $\sigma'(\lambda)$ is called differential absorption cross-section (see Figure 4.3).

$$\begin{aligned} I(\lambda,\sigma) &= I_0(\lambda)\exp\left(-[\sigma_c(\lambda)+\sigma'(\lambda)]\cdot SCD\right) \\ &= I_0(\lambda)\exp\left(-\sigma_c(\lambda)\cdot SCD\right)\cdot\exp\left(-\sigma'(\lambda)\cdot SCD\right) \end{aligned} \tag{4.11}$$

Accordingly the *differential optical density* $\tau'(\lambda,\sigma,\sigma')$ can be determined, which is defined as

$$\tau'(\lambda,\sigma,\sigma') := \ln\left[I(\lambda,\sigma\text{-}\sigma')/I(\lambda,\sigma)\right]. \tag{4.12}$$

In practice $I(\lambda,\sigma\text{-}\sigma')$ is determined applying the similar high pass filter to the measured spectrum.

Combining Equation 4.9 and Equation. 4.12, it follows immediately that

$$\tau'(\lambda,\sigma,\sigma') = \tau(\lambda,\sigma) - \tau(\lambda,\sigma\text{-}\sigma'). \tag{4.13}$$

This is demonstrated also on Figure 4.3. The slant column density of a desired trace species now can now be calculated

$$SCD' := \tau'(\lambda,\sigma,\sigma') / \sigma'. \tag{4.14}$$

The new expression *SCD'* (compared to *SCD* derived from Equation. 4.9) indicates that it is calculated from 'differential' quantities.
In the practical DOAS evaluation process the laboratory spectra of different absorbing trace gases are least squares fitted to the atmospheric spectrum. From the result of the fitting procedure the slant column density can be determined (see section 4.3.2). Because several absorbing trace gases

can be simultaneously detected by their specific spectral absorption features the DOAS method is widely used for atmospheric measurements.

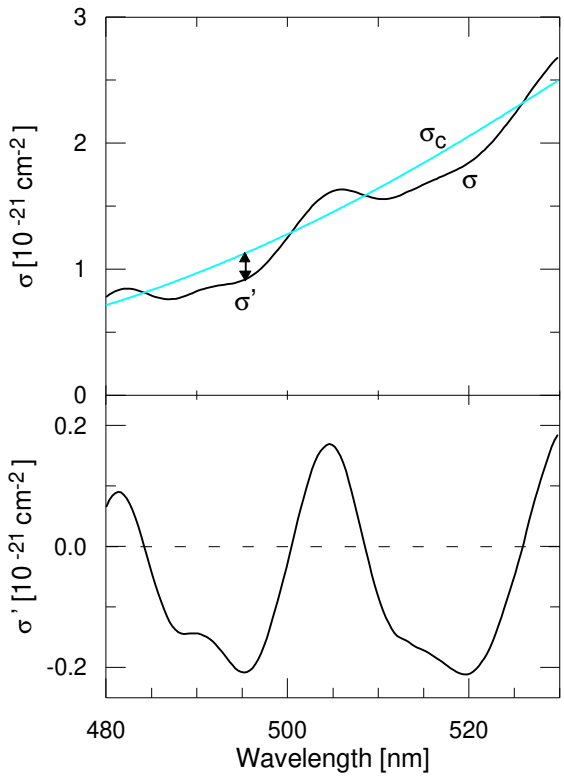

Figure 4.3 Splitting of the absorption cross section into a 'slowly' and 'rapidly' varying part [adapted from Otten, pers. communication].

4.3.1 Application of the DOAS method to the measurement of scattered radiation

The SCD' derived from DOAS observations is usually converted into the vertical column density (VCD), the vertically integrated trace gas concentration. For the observation of direct light from the sun, the moon or stars this conversion is based on the geometric enhancement of the light path compared to a vertical path through the atmosphere. For the measurement of scattered radiation as it is the case for the GOME instrument the light penetrates through the atmosphere via different light paths and the conversion of the SCD' into the VCD is more complex and requires the application of radiative transport models. This aspect is described in more detail in section 5.
Compared to the observation of direct light DOAS measurements of scattered radiation is subject to a more fundamental restriction:
For such measurements the observed intensity is:

$$I_{scatt} = \sum_i I_i = I_0 \sum_i \exp(-\sigma \cdot SCD_i) = I_0 \sum_i \exp(-\tau_i) \qquad (4.15)$$

with τ_i being the optical depth of the absorption path i.
Applying Equation 4.9 to I_{scatt} leads to:

$$\tau_{scatt} = -\ln\left(\frac{I_{scatt}(\lambda,\sigma)}{I_0(\lambda,\sigma)}\right) \neq \sigma \cdot \overline{SCD} \qquad (4.16)$$

with τ_{scatt} the measured optical depth for the scattered light measurement and the $\overline{SCD}$ the average over the individual *SCDs* of all absorption paths contributing to the measured signal. Thus, in general the $\overline{SCD}$ can not be derived from measurements of scattered radiation. Furthermore, it turns out that τ_{scatt} depends of the strength of the cross section, e.g. on the selection of the respective absorption band. This is in particular important because it has to be considered in the radiative transport modelling necessary for the interpretation of the scattered light measurements [Platt et al., 1997; Marquard et al., 1999].
However, for weak absorptions the exponential function (equation 4.15) and the logarithm (Equation 4.16) can be approximated by the first two terms of the Taylor expansions and the $\overline{SCD}$ can be derived from τ_{scatt} in the usual manner (like in Equation 4.9).
It was shown by Marquard et al. [1999] that for scattered light measurements exists in principle a non linear relation between the absorption cross section and the measured optical depth. This is of fundamental importance for the application of the DOAS technique since it is only valid substituting absolute quantities by differential quantities if there exists a linear relationship between τ and σ.
However, since atmospheric DOAS measurements are usually applied to weak atmospheric absorbers the $\overline{SCD}$' determined from the measured τ'_{scatt} is a good approximation for the average of the SCDs of the different absorption paths:

$$\tau'_{scatt} / \sigma' = \overline{SCD}' \approx \overline{SCD} \qquad (4.17)$$

This PhD study deals with the measurement of atmospheric BrO and OClO which are weak atmospheric absorbers (τ < 1% << 1). Thus the difference between $\overline{SCD}$' and $\overline{SCD}$ is very small (below 1%) and thus negligible compared to other uncertainties of the measurements: In the following we will use only the common expression *SCD* when we refer to the measured $\overline{SCD}$'.

4.3.2 The spectral fitting process

The measured spectrum is fitted by the absorption spectra of the trace gases absorbing in the respective spectral range and a polynomial of a specified degree by means of a non linear least squares fitting algorithm [Gomer et al., 1993; Stutz and Platt, 1996]. This fitting algorithm uses the Levenberg-Marquard method [Levenberg, 1944; Marquardt, 1963] which is an iterative combination of a linear part for the retrieval of the trace gas absorptions and a non linear part which accounts for possible spectral shifts between the measured spectrum and the reference spectrum.

Since the spectra are recorded with a diode array of 1024 discrete elements the obtained signal by a single diode represents the integrated intensity over the wavelength range which is covered by this diode:

$$I(\lambda_i) = \int_{\lambda_{i,low}}^{\lambda_{i,high}} I'(\lambda')d\lambda' \qquad (4.18)$$

Here λ_i denotes the centre wavelength of the diode element, $\lambda_{i,low}$ the shortest wavelength and $\lambda_{i,high}$ the longest wavelength covered by the element.
The aim of the linear fitting process is to minimise the sum over the measured optical depths $\tau'(\lambda_i)$ of the individual diode elements of the selected wavelength range:

$$\left| \sum_i \left(\tau'_{meas}(\lambda_i) - \sum_k \alpha_k \cdot \sigma'_k(\lambda_i) - \sum_j \lambda_i^j \right) \right| \rightarrow 0 \qquad (4.19)$$

Here $\sigma_k'(\lambda_i)$ denotes the differential cross section of the k-th trace gas taken into account by the fitting routine. The derived fit coefficient α_k is the desired SCD of this species (sometimes not the cross section of the trace species but the logarithm of an absorption spectrum taken in the laboratory is used in the fitting routine. For this case α_k is the ratio of the desired SCD_k and the SCD_k of the laboratory spectrum). $\sum_j \lambda_i^j$ is a polynomial often used to account for broad band features, e.g. from Rayleigh- and Mie-scattering. In some cases, and in particular in this PhD thesis, this polynomial is used to perform the entire high pass filtering essential for the DOAS technique. Thus, the non high pass filtered cross sections σ' are used in the fitting process instead of the differential ones σ.
In the second part of the fitting process the wavelength calibration of reference spectra is varied with respect to the measured spectrum to achieve the best match of the absorption features in the measured spectrum. For that purpose the reference spectra are interpolated and the grid points λ_i are replaced by the values of the new wavelength $\lambda_{f(i)}$. In this PhD thesis linear shifts and also squeezes of the reference spectra were allowed according to $f(i) = a + b \cdot i$.
The algorithms for the retrieval of the atmospheric trace gases BrO, OClO, O_3, NO_2, O_4, and O_2 from GOME spectra were developed in this work using the evaluation software MFC [Gomer et al., 1993]. After testing and optimising they were implemented in a GOME specific analysis software developed by Leue [1999].
For measurements of scattered solar radiation two further spectra are included in the fitting process: one spectrum to correct the Ring-effect (see below) and another to account for the solar Fraunhofer lines which are the most dominant features in the spectra recorded by GOME. To remove this structures it is a commonly used method (for ground based DOAS measurements) to divide the measured spectra (usually taken at large SZA and thus large atmospheric absorptions) by a spectrum measured at small SZA (and thus small atmospheric absorptions. This spectrum is usually referred to as Fraunhofer reference spectrum). The result of the fitting process then yields the difference of the atmospheric absorptions; thus the absorption of the Fraunhofer spectrum has to be added to derive the total absorption of the measurement. Since the absorption in the Fraunhofer spectrum can often only be derived with relatively large uncertainties, this procedure

represents a specific limitation of DOAS measurements using extraterrestrial light sources (see also appendix A).
In the case of satellite measurements, however, there exists the possibility to record an extraterrestrial spectrum of the solar radiation, which then can be used as Fraunhofer spectrum. Thus it is possible to directly determine the total absorption of a measured spectrum in the fitting process. In practise, usually the logarithm of the Fraunhofer spectrum is simultaneously included in the fitting process.
The difference of the measured optical depth and the result of the fitting routine is called the residual structure (or residual). It is a measure for the quality of the spectral fitting. When the optical depth of the residual is small compared to the a trace gas absorption derived in the fitting procedure the respective trace gas can be well detected. From the random structures of the residual in particular the statistical error for the derived SCDs can be determined [Stutz and Platt, 1996]. Often, however, the residuals contain persistent spectral structures which can be caused by errors in the spectral calibration of the reference spectra, the temperature dependence of the cross sections, or unknown atmospheric absorptions. In addition several further effects arising from scattering processes in the atmosphere, the fine structure of the solar spectrum, and from instrumental artefacts can cause systematic structures (see sections 4.3.7.2 and 4.3.8.2). Such structures have to be considered carefully in order to optimise the spectral fitting procedure and to determine the uncertainty of the derived SCDs [Ferlemann, 1998].

4.3.3 The influence of the spectral resolution of the instrument

The spectral resolution of DOAS instruments in the UV/vis region is usually in the range of about a few tenths to several nanometers. Thus the natural line widths of the atmospheric absorptions are not resolved (see section 4.2). To account for this the absorption cross sections of the trace gases have to be convoluted by the instrumental slit function f(λ) before they are used as input for the fitting routine.

$$\sigma^*(\lambda) = F * \sigma(\lambda) = \int \sigma(\lambda') \cdot f(\lambda - \lambda') d\lambda \tag{4.20}$$

However, it should be noted that in 'reality' this convolution occurs in the spectrometer where the incoming intensity I(λ) is convoluted with the instrument slit function:

$$I^*(\lambda) = F * I(\lambda) = F * I_0(\lambda) \exp(-\sigma(\lambda) \cdot SCD) \tag{4.21}$$

Applying of Equation 4.9 leads to:

$$\tau(\lambda) = -\ln\left(\frac{F * I_0 \exp(-\sigma(\lambda) \cdot SCD)}{F * I_0(\lambda)}\right) \neq F * -\ln\left(\frac{I_0 \exp(-\sigma(\lambda) \cdot SCD)}{I_0(\lambda)}\right) = F * \sigma(\lambda) \cdot SCD \tag{4.22}$$

The convolution and the logarithm or exponential function can not be exchanged. Thus the fitting of convoluted cross sections to the optical depth measured by a low resolving instrument is not strictly correct. Only for an optically thin absorber like atmospheric BrO and OClO ($\tau << 1$) the exponential function and the logarithm can be approximated by the first two terms of the Taylor expansions. And, if also the spectrum of the light source can be approximated by a constant it follows:

$$\tau(\lambda) \approx F * \sigma(\lambda) \cdot SCD \tag{4.23}$$

That means that for small absorptions the measured optical depth is proportional to the SCD. It should be noted that in particular the solar spectrum is not constant with wavelength. As discussed in section 4.1 it is highly fine structured due to the Fraunhofer absorptions of the sun's atmosphere. In some cases this leads to retrieval errors since Equation 4.23 is no longer valid. This effect is often referred to as solar I_0 effect and is described in more detail in section 4.3.5.

4.3.4 The Ring effect

In addition to Rayleigh- and Mie-scattering which are elastic scattering processes in the Earth's atmosphere the solar radiation is also scattered by Raman-scattering whereby the photon's energy changes (see Figure 4.4). Rotational Raman scattering is thought to be the (most probable) cause for the so called 'Filling in' (see Figure 4.5) of the Fraunhofer lines [Bussemer, 1993; Vountas et al., 1998] (and to a lesser degree also of the atmospheric absorption lines [Fish and Jones, 1995]); it was first discovered by Grainger and Ring [1962] and referred to as Ring-effect. Although the Ring effect is only of the order of a few per cent it significantly affects DOAS measurements of scattered radiation: The Fraunhofer lines of the measured spectra can thus not perfectly corrected for by the inclusion of the Fraunhofer spectrum in the fitting process (see section 4.3.4.1). In consequence structures (up to several per cent in the UV spectral range) remain in the residual which mask the weak atmospheric absorptions if the Ring effect is not properly corrected for.
For satellite measurements the impact of the Ring-effect on the retrieval of the trace gas absorptions is even more important than for ground based measurements because a spectrum of direct solar radiation (with no filling-in of Fraunhofer lines) is used as Fraunhofer spectrum and thus the difference of the optical densities of the Fraunhofer lines in the measured spectra and the Fraunhofer spectrum can be much larger than for ground based observations (For the spectral resolution of the GOME instrument up to about 10% in the UV spectral range). Thus a very accurate correction is required, since the atmospheric absorptions which are attempted to be quantified are about more than one order of magnitude smaller compared to the filling in of the Fraunhofer lines.

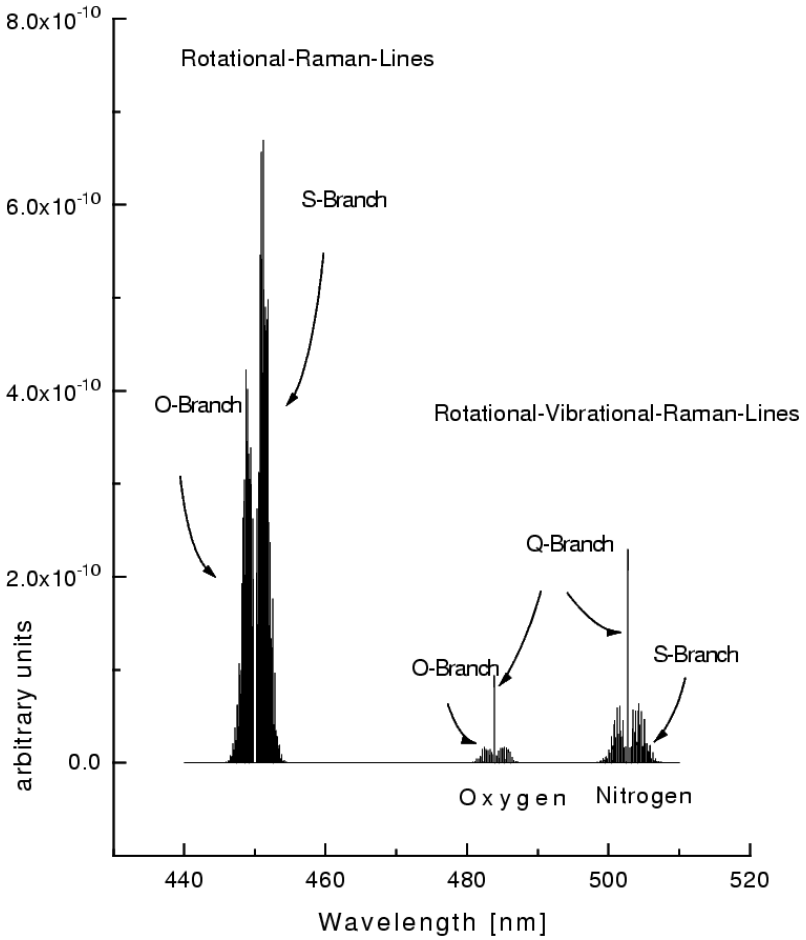

Figure 4.4 Transitions for rotational and vibrational Raman scattering on O_2 and N_2 molecules (adapted from Haug [1996]).

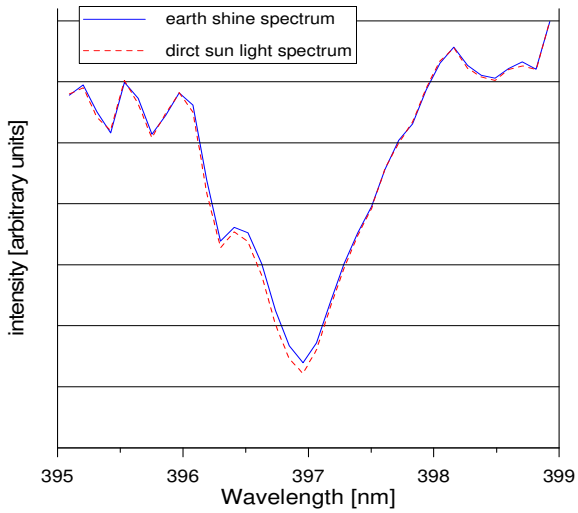

Figure 4.5 GOME spectra of direct solar radiation (9.12.1998) and atmospheric measurement (9.12.1999, 14:57:04, SZA: 82.5°). Compared to the solar spectrum the optical density of the Fraunhofer lines are by about 3 % smaller in the atmospheric measurement.

4.3.4.1 The Ring spectrum

Usually the Ring effect is corrected for by including a further spectrum into the fitting process [Solomon et al., 1987]. The use of the Ring spectrum to correct the 'filling in' of the Fraunhofer lines is based on the assumption that the absorptions of the atmospheric trace gases occur after the Raman scattering has occurred. This is not true for atmospheric measurements because the probability for scattering depends on the air density and increases towards lower altitudes. Thus a large fraction of the atmospheric absorptions (in particular of stratospheric absorbers) can have also already appeared before the photons undergo a scattering process. In consequence the filling in can be expected to occur also for the absorption features of atmospheric species. This effect is usually referred to as 'molecular Ring effect'; in particular for NO_2 it has been demonstrated that it might cause systematic errors up to about 10% [Fish et al., 1995].
In this work the main focus is on the measurement of BrO and OClO and the influence of the molecular Ring effect can be considered to be small compare to other uncertainties (see section 5); thus only the filling in of the Fraunhofer lines was corrected for.
Taking into account a Ring spectrum has proven to be a very successful method to correct for the filling-in in atmospheric measurements of scattered light.
The light I_{meas} detected by the satellite instrument was either scattered in the atmosphere by molecules or aerosols or reflected at the earth's surface. While Rayleigh- and Mie-scattering as well as the reflection are elastic processes, the Raman scattering on molecules introduces an inelastic contribution to the measured light.

$$I_{meas} = I_{elastic} + I_{inelastic} \tag{4.24}$$

To analyse a measured spectrum the negative logarithm of I_{meas} is taken (see section 4.3.4.1).

Since $I_{inelastic}$ is very small (about a few per cent) compared to $I_{elastic}$ the logarithm can be approximated by the first two terms of the Taylor expansion:

$$-\ln(I_{meas}) = -\ln(I_{elastic} + I_{inelastic}) \approx -\ln(I_{elastic}) + \frac{I_{inelastic}}{I_{elatic}} \quad (4.25)$$

with

$$I_{Ring} := I_{inelastic}/I_{elastic} \quad (4.26)$$

I_{Ring} is usually referred to as Ring spectrum and it can be included in the fitting routine to correct the Ring effect. Two common methods exist to derive such a Ring spectrum:

A) Measured Ring spectrum:
This method makes use of the polarisation properties of the different kinds of scattering in the atmosphere. While Rayleigh scattering on air molecules highly polarises the solar radiation (total polarisation at SZA of 90° and a nadir or zenith viewing geometry) rotational Raman scattered light shows only a weak polarisation. From scattered light spectra of different polarisation orientations the rotational Raman scattered intensity can be determined [Solomon et al, 1987b]. However, this method suffers from several shortcomings:
a) Also Mie-scattering enhances the part of depolarised light in the scattered solar radiation. Thus the Ring spectrum determined from the polarisation measurements also contains structures caused by Mie-scattering which does not contribute to the Ring effect.
b) Since the atmospheric paths for light of different polarisation are different they can contain different absorptions of atmospheric trace gases. In consequence a measured Ring spectrum can contain an unknown amount of atmospheric absorptions which affects the retrieval of the trace gas absorptions in the fitting process.
c) Raman scattering shows a weak polarisation of the scattered light. Thus from polarisation measurements the elastically scattered and inelastically scattered parts can not exactly be determined.
d) The measurement of the polarised light spectra refers to specific atmospheric conditions and viewing geometry and was made for the respective properties of the instrument (like wavelength calibration). Since the effort to perform such measurements is rather large only a few measured Ring spectra will be available for the correction of a huge amount of satellite measurements for different measurement conditions. In particular changes of the spectrometer and e.g. the degradation of the instrument cannot be taken into account.

B) Calculated Ring spectrum
From the known energies of the rotational states of the two main gases of the atmosphere, O_2 and N_2, the cross section for rotational Raman scattering can be calculated. This can be done by including Raman scattering into radiative transfer models [Bussemer, 1993; Fish et al., 1995] or by calculating the pure ratio of the cross sections for Raman and Rayleigh scattering. Since the differences between both methods were found to be negligible for the data analysis the Ring spectra were determined by calculating the ratio of the cross sections for Raman and Rayleigh scattering (Y-command of the analysis software MFC [Gomer et al., 1993]. An example for the calculation of a Ring spectrum is shown in Figure 4.7.
Although other authors have found similar or even better results using a measured instead of a calculated Ring spectrum, in this study only a calculated Ring spectrum was used. First, it was found that the filling in could be properly corrected for by this method; in particular when the extended Ring correction method was used (see below). Second, the shortcomings of a measured Ring spectrum are avoided (see above).

4.3.4.2 Sensitivity studies for the correction of the Ring effect

Although it was found that using a calculated Ring spectrum could correct most of the 'Ring structures' in the GOME spectra in particular for the GOME OClO evaluation (see below) it became obvious that in many cases residual structures remained in the fitting process, which were correlated with the structures in the Ring spectrum.
Possible reasons for the insufficient correction of the Ring effect might be:
A) For the appropriate correction of the filling in, the atmospheric radiative transport might have to be modelled more accurate (e.g. taking into account multiple scattering and polarisation).
B) The input parameters for the Raman calculation (temperature, pressure, SZA) might be wrong.
C) The calculation of the Raman spectrum (and thus the Ring spectrum) has to be performed with high spectral resolution and then transformed (convoluted) to the resolution of the GOME instrument. Actually, due to the limited resolution of the GOME direct sun spectrum which is used as input for the Raman calculation the resulting Ring spectrum might not be accurate enough for a proper correction of the filling in.
D) Our method (taking into account a Ring spectrum into the fitting procedure to account for the filling in of Fraunhofer lines) is only an approximation which might find its limitations when the Ring effect is too strong.
E) Especially for satellite observations the detected light is a composition of photons scattered and reflected by mechanisms (Rayleigh scattering, Mie-scattering, reflection on the Earth's surface) which have different broad-band wavelength dependencies. Applying Equation 4.26 this leads to a modulation of the Ring spectrum which might differ strongly from measurement to measurement, due to changes of the conditions of the atmosphere (aerosol load and clouds) and the ground albedo.
We investigated most of the above points (except point D) and it turned out that point A, B and C had only weak influence on the quality of the fitting results. As an example Figure 4.6 shows the dependency of the residual structure of a GOME OClO evaluation when the temperature used for the Raman calculation is varied.

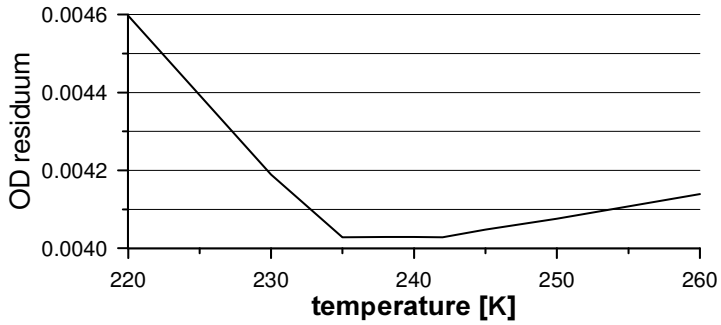

Fig. 4.6: Dependence of the magnitude of the residual structures (optical densities) of the GOME OClO evaluation (a spectrum with very large Ring effect was used, #117 of GOME orbit 70113021, optical density of the Ring effect: 7.7%) on the temperature used for the calculation of the Ring spectrum. Only a very weak temperature dependence was found.

4.3.4.3 An advanced concept for the correction of the Ring effect

It turned out that for many cases point E) (see section 4.3.4.2) appears to be of great importance, especially if a relatively large wavelength range is used for the spectral analysis e.g. as for the OClO evaluation. To further investigate this aspect the standard OClO DOAS evaluation (see

section 4.3.8) was modified taking into account two Ring spectra instead of only one (see Fig. 4.7). The first Ring spectrum was the original one which was calculated under the assumption that Rayleigh scattering contributes the largest part to the elastically scattered light. The second Ring spectrum was calculated assuming that the light was reflected from the (grey) surface of the earth. Both spectra are expected to describe two extreme cases. Typically also Mie-scattering contributes to the elastically scattered light and the appropriate Ring spectrum should lie in between both extreme cases.
Especially for the GOME OClO evaluation which uses a wide wavelength region in the UV, this method lead to significant smaller (up to 35%) residual structures and thus smaller fitting errors compared to the standard evaluation (see Fig. 4.8). However, the retrieved OClO absorptions when using two Ring spectra were nearly the same (a relative difference up to about 5%) as for the standard evaluation.
As a side product of this new method for the correction of the Ring effect it might be possible to determine the different contributions of the scattering and reflecting mechanisms to the detected light. This could therefore lead to a new method to retrieve information about e.g. the cloud cover, ground albedo etc..

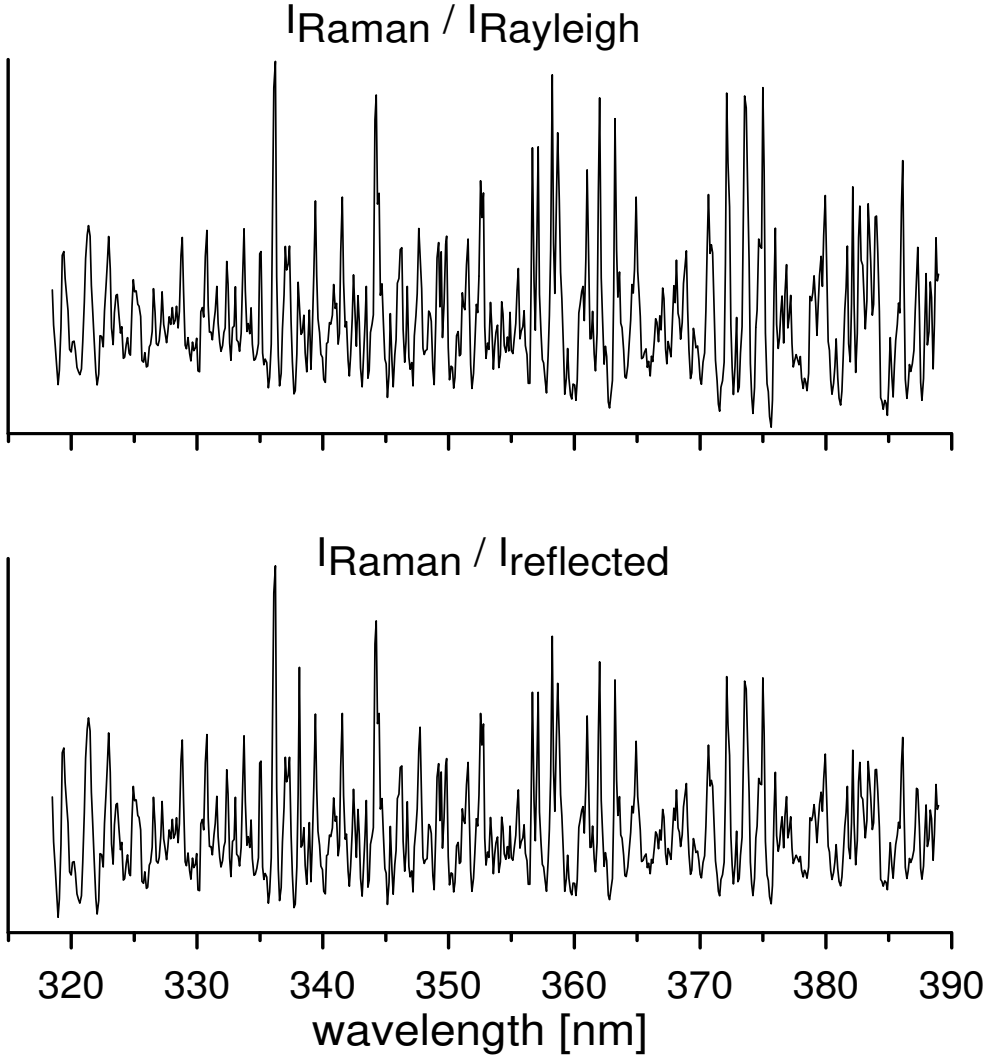

Fig. 4.7: Top: Original Ring spectrum taking only Rayleigh scattering into account. Bottom: Second Ring spectrum calculated for light reflected on the (grey) earth's surface.

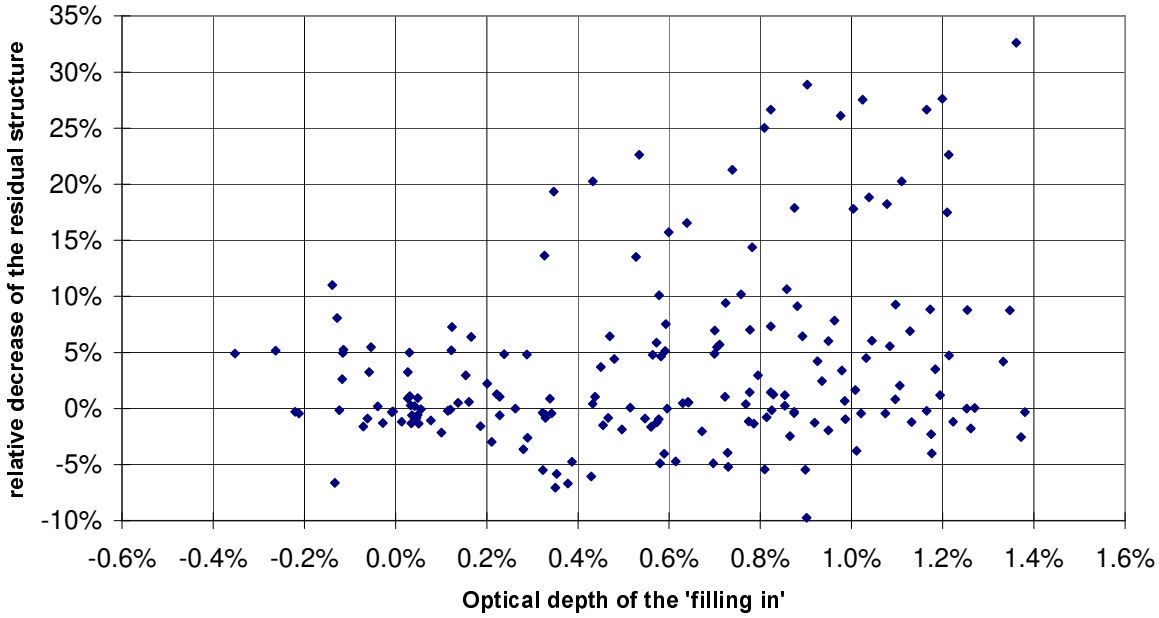

Fig. 4.8: Relative difference in the magnitude of the residual structures between the standard GOME OClO evaluation and the new evaluation using two Ring spectra as a function of the strength of the Ring effect. For most of the spectra the residual structures of the fitting procedure were significantly reduced compared to the standard evaluation.

4.3.5 The 'solar I_0-effect'

Because of the large number of Fraunhofer lines the intensity of the solar spectrum varies strongly with wavelength. Thus the approximation which leads to Equation 4.21 are not fulfilled. In particular for absorptions showing also narrow spectral structures the absorptions found in measured atmospheric spectra can not be fitted properly by the respective cross sections (which are usually measured in the laboratory using a light source with a smooth spectrum, e.g. a black body radiator). Because these errors arise from the spectral structures of the I_0 spectrum it is usually referred to as solar I_0 effect [Paul Johnston, pers. comm.; Platt et al., 1997, Friess, 1997; Richter, 1997; Van Roozendael et al., 1999b]. While for most of the atmospheric absorbers this leads only to negligible effects in some cases the I_0 effect has to be considered. This is in particular the case when strong atmospheric absorbers like O_3 have to be 'removed' to measure the underlying weak absorptions of other trace gases like BrO. The solar I_0 effect can be accounted for using so called 'I_0 corrected' cross sections. These can be calculated in the following manner: First the highly resolved solar spectrum $I_0(\lambda)$ is convoluted with the instrument slit function:

$$I_0^*(\lambda) = F * I_0(\lambda) \tag{4.27}$$

In the next step the absorption spectrum of the chosen trace gas (calculated with a highly resolved cross section and solar spectrum) is convoluted with the instrument slit function:

$$I^*(\lambda) = F * [I_0(\lambda) \cdot \exp(\sigma \cdot SCD)] \tag{4.28}$$

The I_0 corrected cross section is then derived:

$$\sigma_{corrected}(\lambda, SCD) = -\ln\left(\frac{I^*(\lambda)}{{I_0}^*(\lambda)}\right) \tag{4.29}$$

Clearly I_0-corrected cross sections derived in this manner can perfectly match the absorptions in the measured atmospheric spectrum only if the same SCD was used for the calculation which appeared in the atmosphere. However, it turned out that this was not a critical point and the I_0 corrected cross sections could be used for a large range of atmospheric SCDs. For improved DOAS analysis an iterative approach could be applied using the SCDs retrieved in a first fitting process to calculate I_0 corrected cross sections of several absorbers. These could be used for the next DOAS fitting and so on.
It was shown e.g. by Van Roozendael et al. [1999b] that for ground based measurements of BrO at mid latitudes in summer the derived BrO absorption is effected by up to 30% if the simultaneously fitted O_3 cross sections are I_0 corrected or not. In contrast, for BrO measurements at polar regions, in particular in winter time, the influence of the I_0 effect on the BrO analysis was found to be much smaller. This might be mainly caused by two effects: first the BrO SCD for such conditions is much larger than at mid latitudes. In addition, the stratospheric O_3 absorptions occur on significantly lower temperatures leading to smoother spectral features of the strong temperature dependent O_3 cross section in the UV spectral range. Also for GOME measurements of BrO the solar I_0 effect was found to be in the range of only a few per cent [Van Roozendael, pers. comm.; Richter, pers comm.]. This is by far smaller than the errors introduced by other effects (see sections 4.3.7.2 and 4.3.8.2); thus the correction of the solar I_0 effect was not taken into account in this PhD thesis.

4.3.6 Instrumental shortcomings and their consideration

4.3.6.1 Fabry Peron etalon structures

There are several effects which influence the spectral transmission function of the instrument. Most of them like the reflectivity of the mirror or the quantum efficiency of the photodiode array are assumed to be constant with time. Even if they cause errors in the absolute radiometric calibration this is only of minor importance because such effects cancel out when the measured spectrum is divided by the Fraunhofer spectrum. However, there exist also other effects like the transmission of the dichroic filter (used as channel seperator, see Figure 3.2) or the etalon structure due to water ice on the surface of the photodiode array which can vary with time. Although they are corrected for according to the measurements of the GOME calibration unit in some cases (e.g. after power shut down) the changes can be very rapid and spectral structures remain which can interfere with the trace gas absorptions.

4.3.6.2 Undersampling of GOME spectra

Due to the low sampling ratio (number of pixels per FWHM of the instrument function, see Roscoe et al. [1996]) of the GOME instrument (2 to 3) the GOME DOAS evaluation is very sensitive to changes of the characteristics of the instrument. While the evaluation software can in principle compensate for shifts of the wavelength calibration of the measured spectra in the case of undersampled spectra information is lost due to the interpolation of the spectra. Fortunately it

turned out that (at least in the UV where the BrO and OClO absorptions are measured) the GOME instrument is very stable with respect to spectral shifts. During one orbit the maximum shift in wavelength is in the order of about 0.02 pixel (about 0.002 nm, see Fig. 4.9) and thus the interpolation errors were found to be very small.

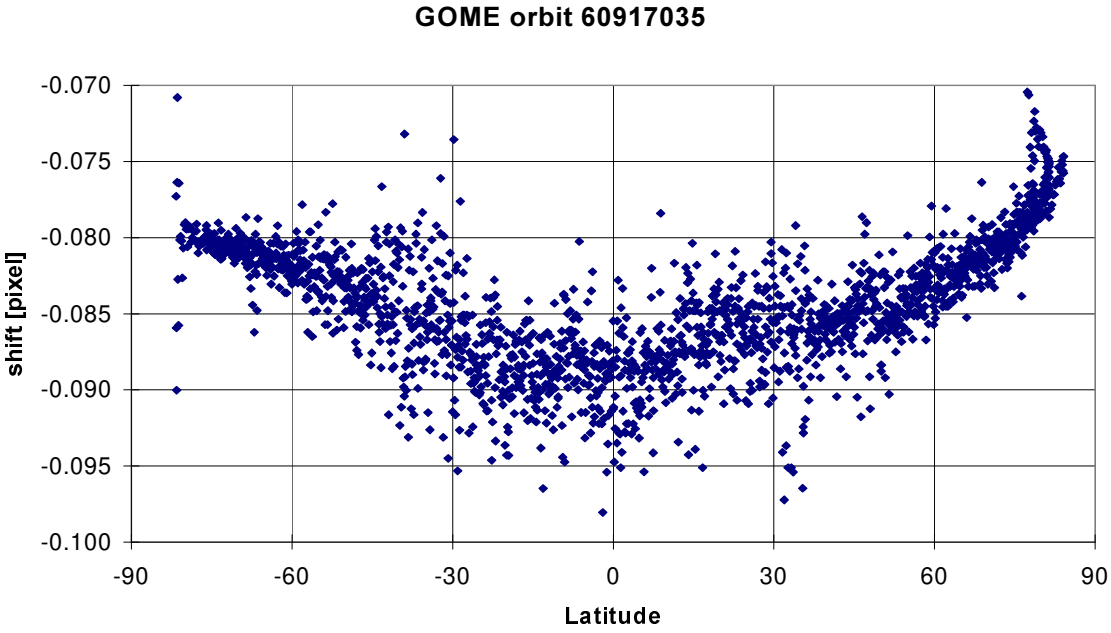

Fig. 4.9: spectral shifts of the wavelength calibration of the measured spectra during one orbit with respect to a GOME spectrum of direct sun light.

4.3.6.3 Doppler shift

If a direct sun light measurement is used as Fraunhofer spectrum the interpolation errors are large. It was found that there appear systematic structures of about more than one per cent which are larger than the atmospheric absorptions of BrO and OClO. It turned out that the most probable cause for it is a shift in the wavelength calibration for the direct solar spectra compared to the Earth shine spectra due to the Doppler effect due to the relative velocity between the spectrometer and the sun during the measurement of the direct sun spectra [Richter, pers. comm.; Van Roozendael, 1999c]. The direct sun spectra are usually recorded when the satellite turns from the dark back side of the Earth to the bright day side. During this part of its orbit the satellite moves with a velocity of about 6.7 km/s towards the sun with respect to the Earth's surface causing a Doppler shift of about 0.008 nm. It was possible to simulate these residual structures (see Figure 4.10) [K. Chance; A. Richter, M. Van Roozendael, personal communication] and to include them in the fitting process. In consequence the residual structures could be strongly reduced. However, it turned out, that in many cases residual structures of about 0.5 % remained. In addition, it was found that the results of the derived trace gas absorption depended on the assumptions which were used to calculate the correction spectrum.
The residual structure shows high frequency structures (pixel to pixel variability), which are narrower than the instrument's slit function and in particular much narrower than the BrO and OClO absorption structures. In this work we 'removed' them applying a low pass filter (Gaussian shape, FWHM: 2.5 pixel). This filter reduces the residual structure by about one order of magnitude while the spectral information about the atmospheric trace gas absorptions is hardly

affected. As a positive side effect the numerical fitting routine was found to be more stable and faster when the spectra are smoothed. From a comparison with other algorithms which also take the simulated structure into account it turned out that the results of both methods were very close to each other (see section 4.3.7.2.4).

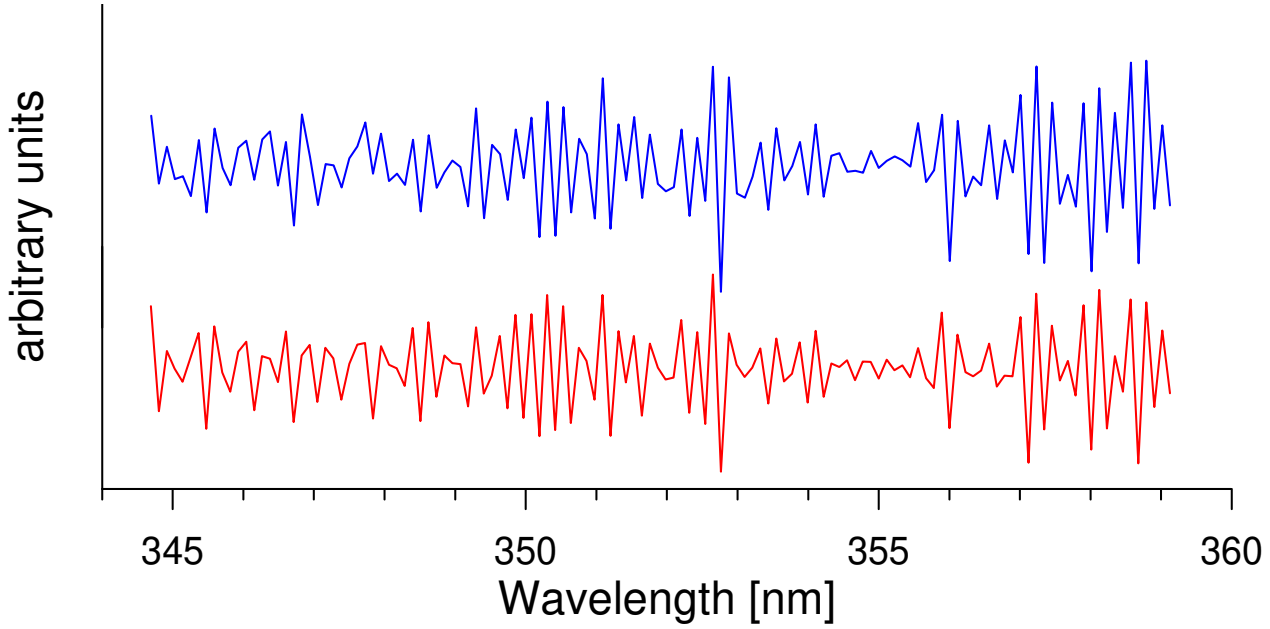

Figure 4.10 Residual structures appearing if a GOME measurement (Earth shine spectrum) is analysed using a direct sun light measurement as Fraunhofer spectrum (upper panel). In the lower panel a simulation of this structure is shown; it was calculated by A. Richter (pers. communication). For that purpose a highly resolved Fraunhofer spectrum is convoluted by the instrument slit function and sampled at a slightly shifted wavelength grid compared to the GOME Earth shine spectra [Chance et al., 1998]. If this spectrum is shifted back to match the wavelength grid of the original Earth shine spectra, relatively large interpolation errors appear. Subtracting the shifted spectrum from a spectrum sampled at the wavelength grid of the Earth shine spectra leads to the residual structure which is very similar to the structures found in the fit of the GOME spectra. Although the overall GOME residual structure is very good reproduced, there appear still differences. Since the optical density of the residual structure is up to about 2 %, still large structures remain relatively even when the modelled structure is included in the fitting process.

4.3.7 Development of the BrO analysis for GOME spectra

4.3.7.1 Wavelength range and reference spectra

The BrO molecule shows a pronounced spectral structure at wavelengths below 365 nm. For the measurement of scattered light it is difficult to use the spectral regions below 340 nm because the ozone absorptions are getting large which affects several approximations only valid for small absorptions (see section 4.3). In particular, also the AMF for BrO shows spectral features [Marquard et al., 1999] (see also section 5.2) which influence the fitting procedure. It turned out that for the BrO analysis of GOME spectra the wavelength range between 344 and 359 nm is best suited. This wavelength range was in particular recommended by Van Roozendael et al. [1999].

Reference spectra of NO_2, BrO, OClO, O_4 and O_3 (two temperatures) were used in the spectral fitting process. The Fraunhofer lines and the Ring effect were corrected for by simultaneous consideration of a direct solar spectrum (as close as possible to the measured spectra, typically observed at the same day) and a calculated Ring spectrum (see section 4.3.4), respectively. Since the wavelength range for the BrO analysis is rather small, only one Ring spectrum was used here. To account for broad band effects like Rayleigh and Mie-scattering a polynomial of degree two was considered in the spectral fitting process. This set of parameters was also recommended by the study of Van Roozendael et al. [1999b] in which the author of this PhD thesis was also involved. The measured spectra and the cross sections are smoothed by convoluting with a Gaussian function with a FWHM of about 2.5 pixel. The spectral calibration of the reference spectra was performed in two steps: In a first step the absolute wavelength calibration given by the authors of the cross sections and provided by the spectral calibration of the GOME spectra was used. In a second step the relative wavelength calibration of the individual cross sections with respect to the measured spectra was optimised by investigating the spectral shifts for large atmospheric absorptions. In particular for the BrO cross section it turned out that the wavelength calibration given by Wahner et al. [1988] must be corrected by about 0.21 nm to match the atmospheric BrO absorptions measured by GOME (see Figure 4.11).

Reference spectrum	temperature	Source
O_3	221 K	GOME [Burrows et al., 1999]
O_3	241 K	GOME [Burrows et al., 1999]
NO_2	227 K	GOME [Burrows et al., 1998]
OClO	203 K	Wahner et al. [1987]
BrO	227 K	Wahner et al. [1988]
O_4	296 K	Greenblatt et al. [1991]
Calculated Ring spectrum	250 K	MFC, Bussemer [1993]
Fraunhofer spectrum	-	GOME direct sun light

Table 4.1 Reference spectra used for the GOME BrO analysis.

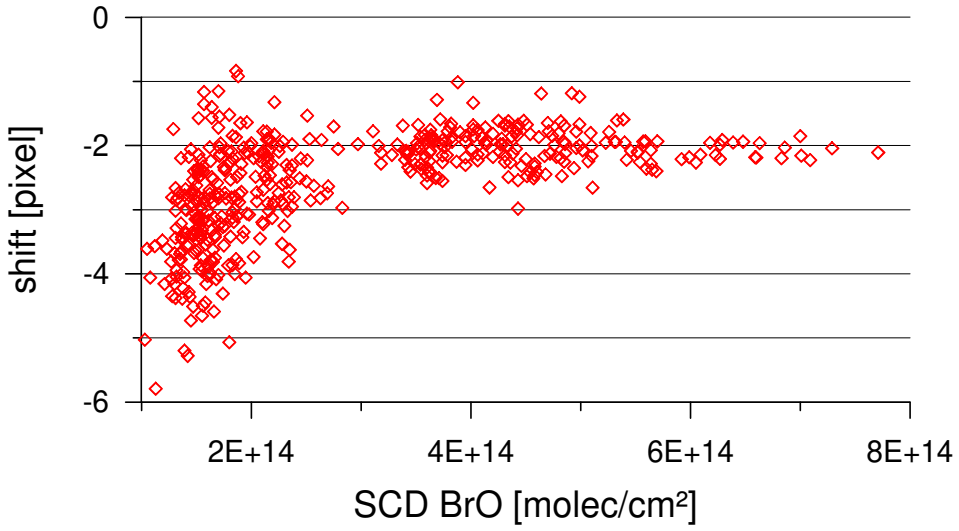

Figure 4.11 Spectral shift of the BrO cross section with respect to GOME spectra as a function of the determined BrO absorption (one pixel equals 0.1 nm). For large BrO absorptions a spectral shift of about 0.21 nm was determined.

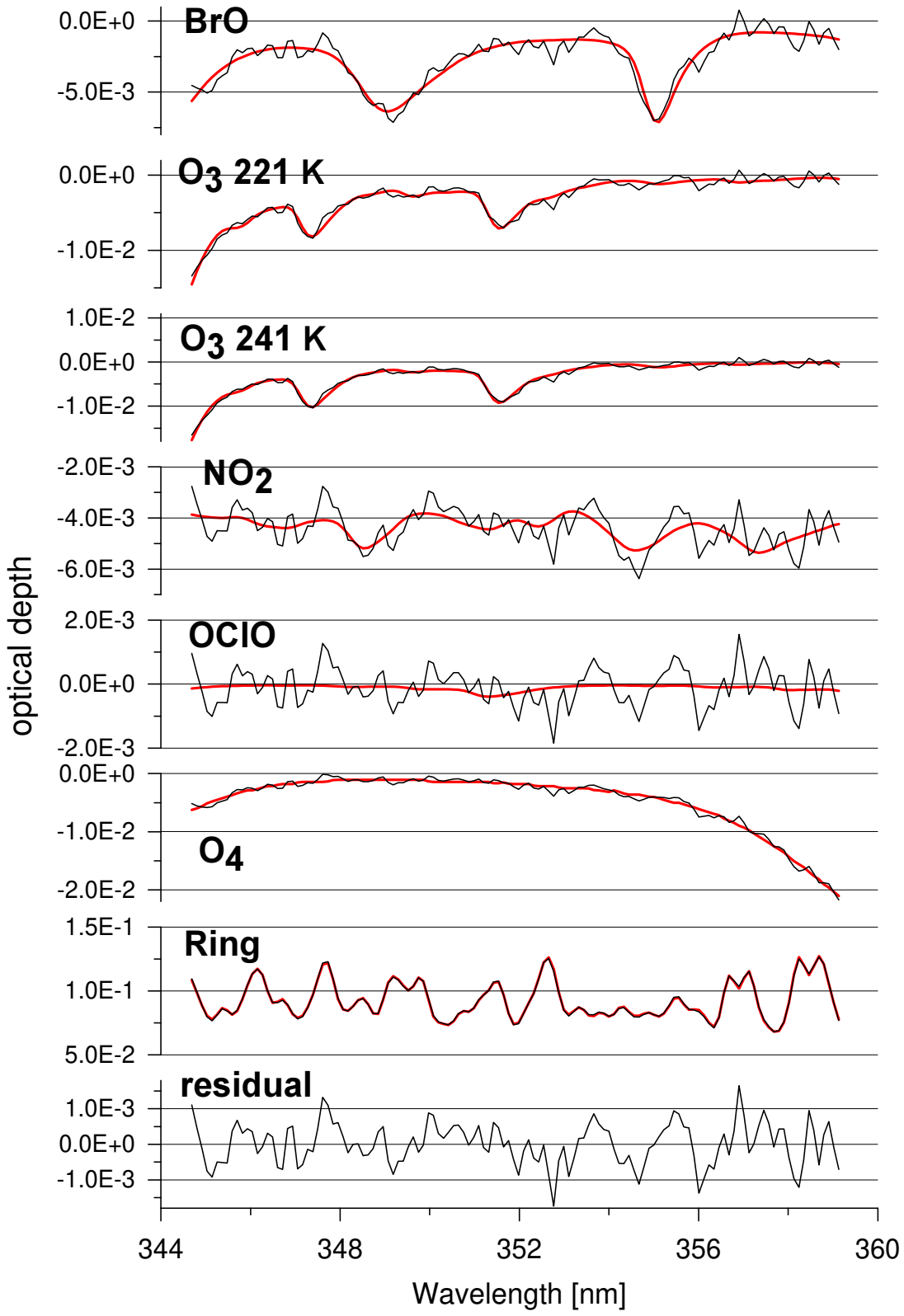

Figure 4.12 Example for the BrO evaluation of an atmospheric GOME spectrum (orbit 60915214, ground pixel #1957). The thick lines indicate the trace gas absorption spectra scaled to the respective absorptions retrieved from the GOME spectrum (thin lines).

Once the wavelength calibration of the reference spectra is determined (with respect to the Fraunhofer spectrum used in the fitting process) the shift of these spectra is 'linked' to the shift of the Fraunhofer spectrum relative to the measured spectrum[2]. Since the Fraunhofer lines are the dominating features in both the measured and the Fraunhofer spectrum due to this performance unreasonable shifts of the reference spectra, in particular for weak absorptions are avoided. Table 4.1. summarises the reference spectra used in the BrO fitting process.
In Figure 4.12 and 4.13 examples of the spectral fitting of the BrO absorption in GOME spectra are shown which demonstrate that BrO can clearly be detected by GOME. This GOME observation was made during an event of enhanced tropospheric BrO concentrations in Antarctic spring (see section 6.2) which causes high BrO absorptions while the other atmospheric absorbers, in particular stratospheric O_3 show only moderate absorptions due to the relatively small SZA. Under such conditions, the wavelength dependence of the AMF is rather small (see section 5) and the wavelength range for the BrO analysis can be extended towards smaller wavelengths where an additional absorption band of BrO can be used.

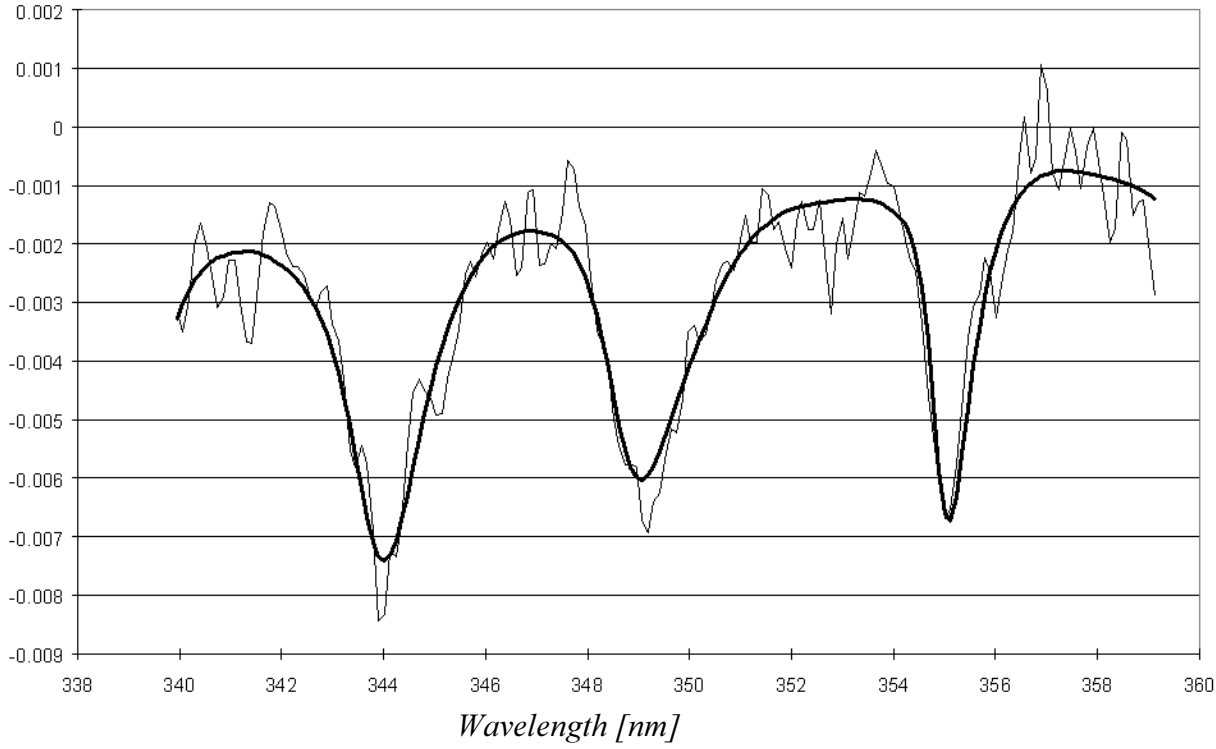

Figure 4.13 Under the specific conditions of the GOME measurement shown in Figure 4.12 (large BrO absorption due to enhanced tropospheric concentrations but low O_3 absorptions due to only moderate SZA) the BrO absorption can be clearly detected also in a larger spectral window containing 3 BrO absorption bands. For the standard BrO retrieval the wavelength region from 344.8 to 359 nm is used because the spectral analysis at wavelengths below about 344 nm is strongly affected by the wavelength dependence of the AMF due to the strong O_3 absorption (see section 5.2).

[2] The spectral shift (and squeeze) determined for the Fraunhofer spectrum is also applied to the other spectra used in the DOAS fitting.

4.3.7.2 Determination of the fitting error for the BrO evaluation

The error analysis was performed using the method of Stutz and Platt [1996]. This includes two contributions: First, the error of the linear part of the spectral fitting procedure which can be determined from the differences between the measured spectrum and the result of the linear fit and second the error which is caused by the uncertainty of the spectral calibration of the various reference spectra used in the fitting process.
While both errors have statistical contributions due to the noise of the measured spectra and the statistical variations of the determined shift during the fitting routine, there occur also systematic errors (e.g. a wrong wavelength calibration or the undersampling problem) which lead to systematic structures in the residual. The different contributions to the total errors were investigated for different measurement conditions by applying three different methods.
First the statistical error of the spectral fitting process is determined from the residual structure. In a second step the impact of the undersampling problem of GOME on the BrO retrieval is investigated. Finally the influence of spectral shifts of the different cross sections on the BrO analysis is investigated. The selected atmospheric conditions include:
a) GOME BrO measurement at small SZA and thus weak BrO absorptions: Ground pixel #1601 of orbit 60915214, 15.09.1996.
b) GOME BrO measurements at moderate SZA but enhanced tropospheric BrO concentrations. For these conditions the BrO absorption are strong compared to the other atmospheric absorptions: Ground pixel #1957 of orbit 60915214, 15.09.1996.
c) GOME BrO measurements at large SZA; thus the BrO absorptions but also the other atmospheric absorptions are large due to the long stratospheric absorption path: Ground pixel #1601 of orbit 60915214, 15.09.1996.
These three pixels were also chosen for an early intercomparison study of GOME BrO algorithms initiated by the author in Heidelberg in December 1996. Since then, they were often used by various groups (see below).

4.3.7.2.1 Determination of the statistical error of the fitting process.

Due to the undersampling problem of GOME there appear large systematic residual structures if a measurement is analysed using a spectrum of direct sun light. To minimise the impact of these structures on the BrO retrieval the spectra were smoothed by a convolution with a Gaussian function of about 2.5 pixel FWHM. Because of the presence of the systematic residual structure and the application of the spectral smoothing the error calculated from the fitting algorithm cannot be used as the true statistical error of the linear fit because this relation is only valid for purely statistical residual structures [Stutz and Platt, 1996]. Therefore, the statistical error of the linear fit was derived using an Earth shine spectrum measured at a small SZA as Fraunhofer spectrum. In this case the systematic structure does not appear and the error given by the linear fit can be regarded as statistical error (for this determination the spectra were not smoothed, see Figure 4.14). In the next paragraph we will show that despite a constant offset (which is expected due to the BrO absorption in the Earth shine Fraunhofer spectrum) there appears no significant discrepancy between the results achieved with the different Fraunhofer spectra (direct sun light or Earth shine spectrum). Knowing this we can conclude that the systematic residual structure has only a negligible effect on the BrO analysis of GOME spectra (if the spectra are smoothed).
The statistical errors of the linear part of the fitting process were found to be about 19 % for the pixel #1601, about 4% for the pixel #1957 and about 7% for the pixel #2138.

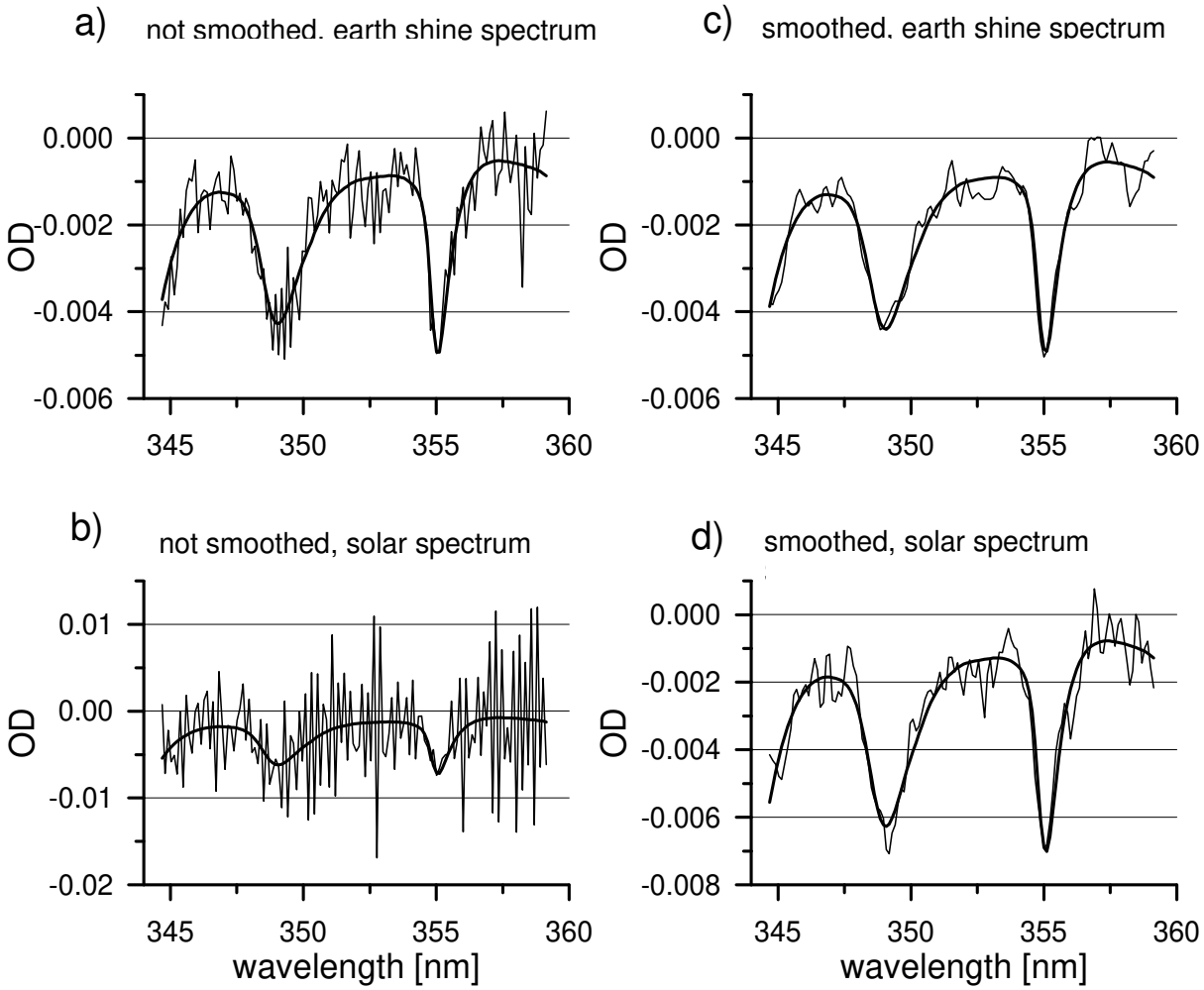

Fig. 4.14 Results of the spectral retrieval of the BrO absorption in a GOME spectrum using different Fraunhofer spectra and with or without smoothing the spectra.

4.3.7.2.2 Impact of the undersampling problem of GOME on the BrO analysis

Since the systematic residual structure shows very narrow variations (from pixel to pixel) it can be expected that the spectral interference with the much wider atmospheric absorption features should be rather small. To investigate this in more detail the measurements of part of one orbit (60916214) were evaluated using different conditions: with and without smoothing and/or using different Fraunhofer spectra (as for the cases presented in Figure 4.14). The results of these evaluations as well as their differences are presented in Figure 4.15. From the comparison of these results the following conclusions can be drawn:

a) The difference between the evaluations with smoothed/unsmoothed spectra is smaller than the statistical uncertainty calculated by the fitting procedure.

b) It is nearly constant for the whole orbit shown in Fig. 4.15.

c) The retrieved BrO absorptions using an earth shine spectrum as a Fraunhofer reference are systematically smaller (as expected) than using a direct sun spectrum.

d) The difference is nearly constant for the whole orbit shown in Fig. 4.15.

From these findings we conclude that the impact of the systematic difference between earth shine and direct sun light spectra from GOME is negligible when the spectra are smoothed before the

fitting process. These conclusion is confirmed also by the results of other groups (A. Richter, personal communication).

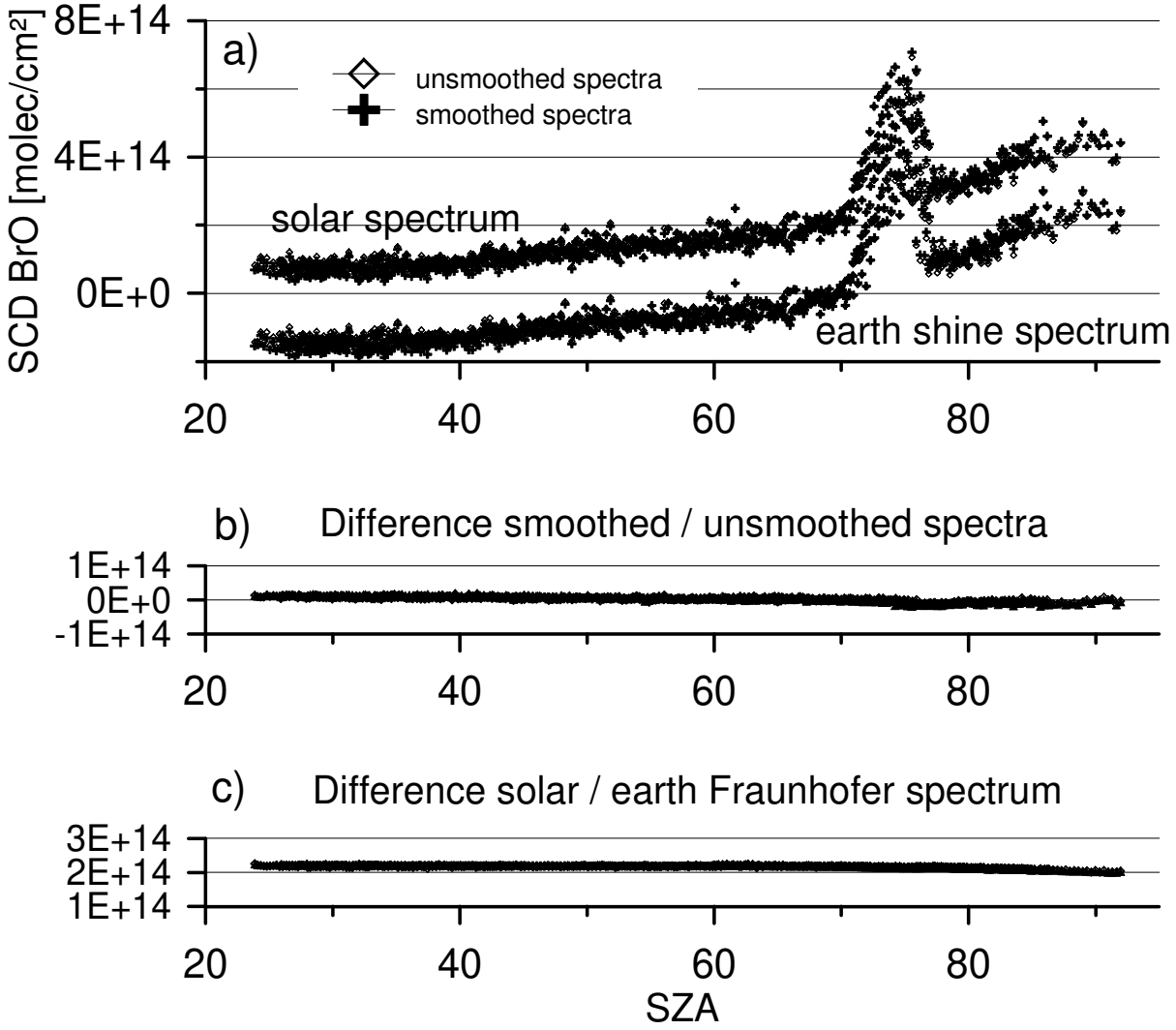

Fig. 4.15: Results of the different evaluations (see also Fig. 4.14) for the orbit 60715214 at 15.09. 1996 are shown in panel a) as a function of the solar zenith angle. The differences between the results of the evaluation using smoothed or unsmoothed spectra are presented in panel b), the differences between the results using different Fraunhofer references in panel c). When a direct solar spectrum is used as Fraunhofer spectra the determined BrO SCD is higher by a constant offset compared to the use of an earth shine spectrum. This is due to the amount of BrO absorption in the Earth shine spectrum. Smoothing of the spectra has only negligible effect on the retrieved BrO SCD.

4.3.7.2.3 Errors caused by uncertainties of the wavelength calibration

Another source of error arises from the uncertainty of the wavelength calibration of the different spectra used in the fitting procedure. To quantify this error a test was carried out according to the method suggested by Stutz and Platt [1996]. The dependence of the fitted BrO SCD on shifts in the wavelength calibration of several reference spectra used in the fitting procedure is investigated (see Figures 4.16 a - c).

It can be seen that for pixel #1601 and #2138 the derived BrO absorption depends strongly on shifts of the O_3 cross sections and the Ring spectrum. For the pixel #1957 it depends mostly on shifts of the BrO reference itself which can be expected because of the enhanced BrO absorption for this measurement.
From the uncertainty of the wavelength calibration the resulting influence on the BrO analysis can now be determined. For the Ring spectrum no uncertainty of the shift (relative to the Fraunhofer spectrum) appears because it is calculated from the respective Fraunhofer spectrum used in the BrO analysis. The uncertainty of the wavelength calibration is about ± 0.2 pixel for O_3 and NO_2, and about ± 0.4 pixel for OClO, O_4 and BrO. The single errors caused by the uncertainties of the different cross section are added square. The resulting error due to the uncertainties in the wavelength calibration was found to be about 12 % for pixel #1601, about 4% for pixel #1957 and about 10% for pixel #2138.

4.3.7.2.4 Total error of the GOME BrO analysis

The results of the error analysis are summarised in Table 4.2. The total error is derived by the square addition of the individual errors of the linear and the non linear part of the fitting process.

Ground pixel	properties	error of the linear part of the fitting process	error due to uncertainties of the wavelength calibration	resulting error (error of cross section not included)
#1601	45.4° SZA, weak BrO absorption	19 %	12 %	24 %
#1957	75.6° SZA, strong BrO absorption	4 %	4 %	6 %
#2138	90.6° SZA, strong BrO absorption	7 %	10 %	12 %

Table 4.2 Errors of the BrO analysis of GOME spectra for different conditions of the measurements. The error of the cross section is not included, see text.

The high precision of the GOME BrO analysis developed in this study is also confirmed by the results of a comparison study with other groups (Figure 4.17).
It should be noted that the uncertainty of the BrO cross section given by Wahner et al. [1988] can lead to a systematic error of about 8%. This error has also be taken into account when absolute BrO measurements from GOME (or other DOAS measurements) are compared to BrO data from other observations. However, this error does not influence conclusions which are based on relative comparisons of GOME BrO measurements such as the observed increase of the BrO absorption due to enhanced tropospheric BrO concentrations (see section 6.3).

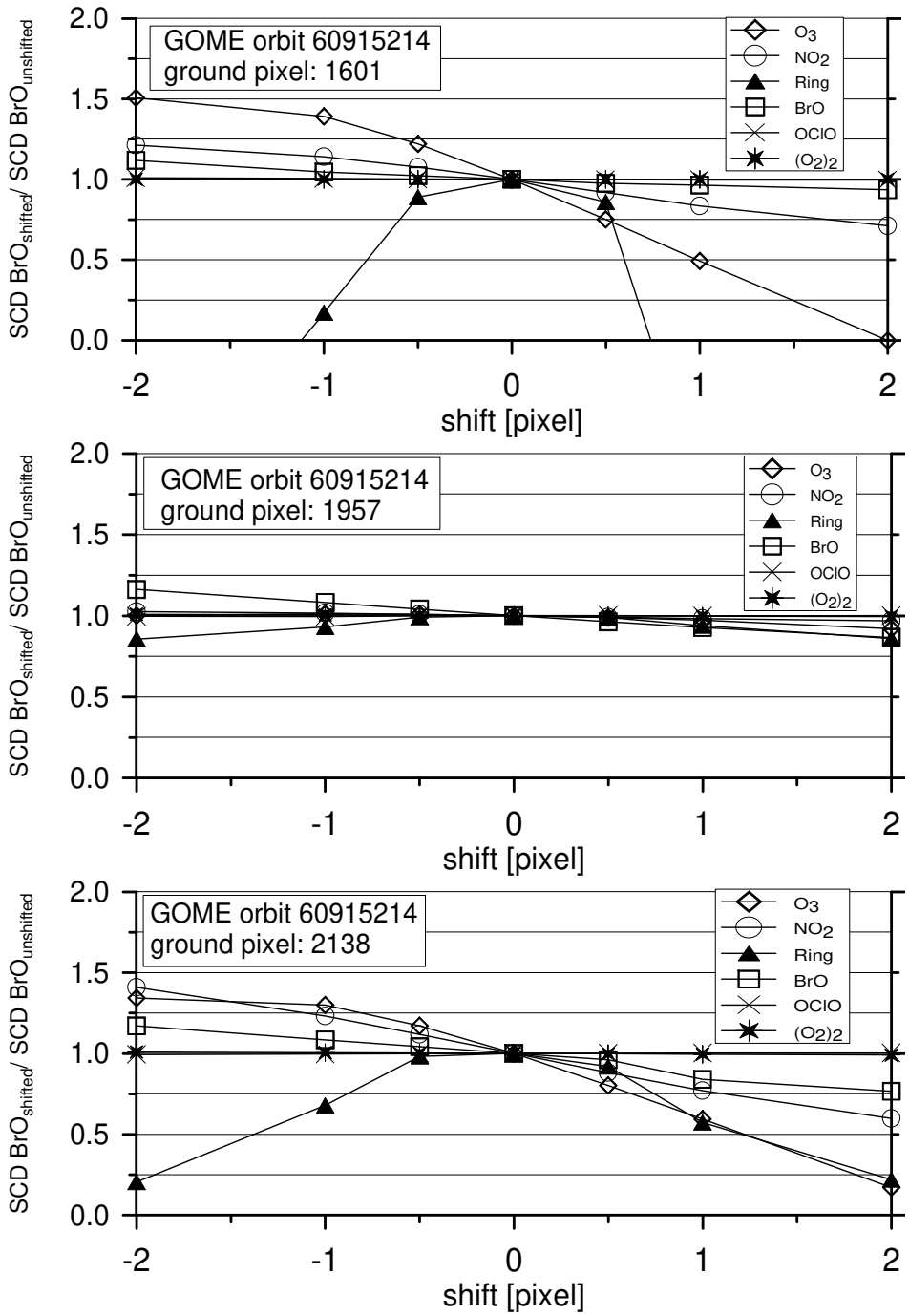

Fig. 4.16 Dependence of the BrO SCD on shifts in the wavelength calibration of the reference spectra used in the fitting procedure for the three selected ground pixels of GOME orbit 60915214.

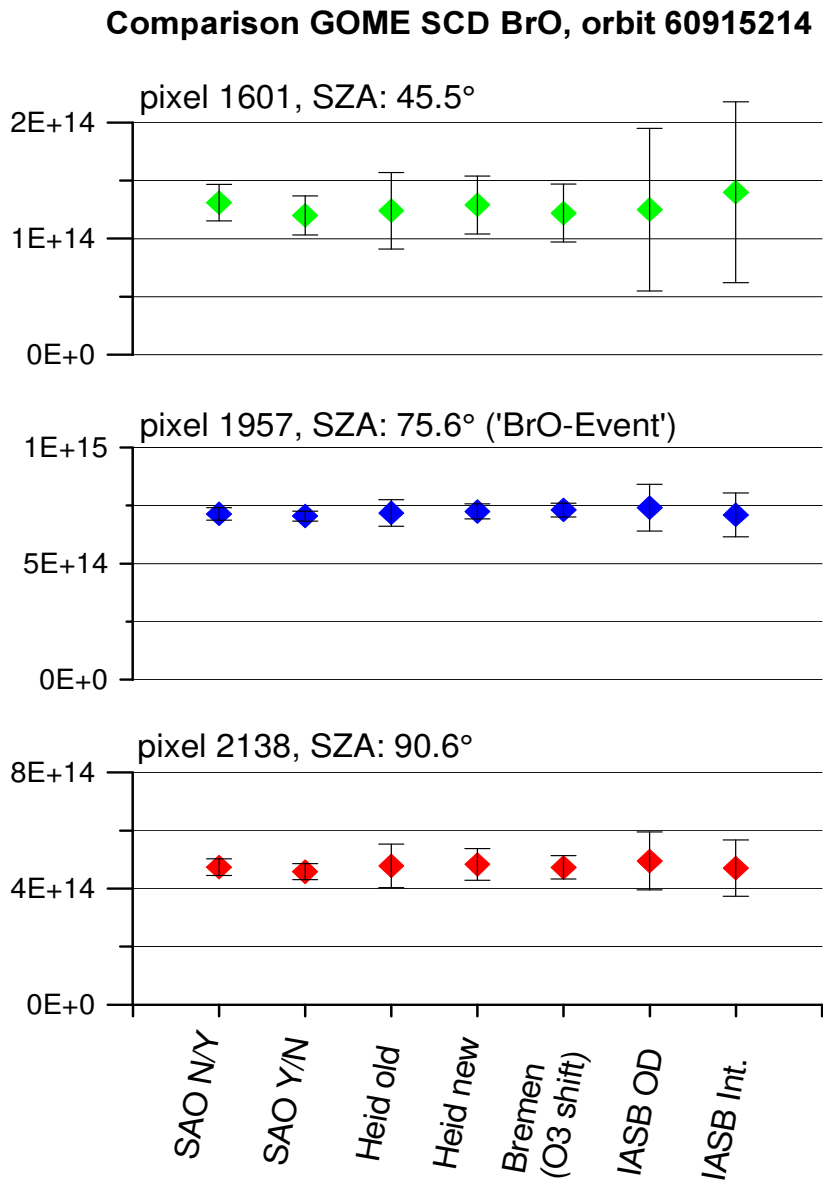

Figure 4.17 Comparison of the GOME BrO analysis of different groups and different algorithms for the selected ground pixels. These results were presented by the author of this PhD thesis at the ESAMS meeting (European Symposium on Atmospheric Measurements from Space) in January 1999 at ESTEC (EUROPEAN SPACE RESEARCH AND TECHNOLOGY CENTRE), Noordwijk, The Netherlands [Wagner et al., 1999a].
SAO: Harvard-Smithsonian Center for Astrophysics, Cambridge Massachusetts, K. Chance, pers. comm.; N/Y: Spectra were not smoothed, an average residual structure was included in the fitting procedure, Y/N: Spectra were smoothed, no average residual structure was included in the fitting procedure.
Heid: Instutitut für Umweltphysik, University of Heidelberg, results of this PhD thesis; old: first BrO analysis algorithm (beginning of 1997), new: Evaluation using an improved Ring spectrum (since summer 1998).
Bremen: Instutitut für Umweltphysik, University of Bremen, A. Richter, pers. comm.
IASB: Belgian Institute for Space Aeronomy (IASB-BIRA), M. Van Roozendael, pers. comm.; OD: fitting of optical densities, int: fitting of intensities [Chance, 1998].

4.3.8 Development of the OClO algorithm for GOME spectra

4.3.8.1 Wavelength range and reference spectra

OClO shows characteristic absorption features over a large wavelength range below 430 nm (Figure 4.18).

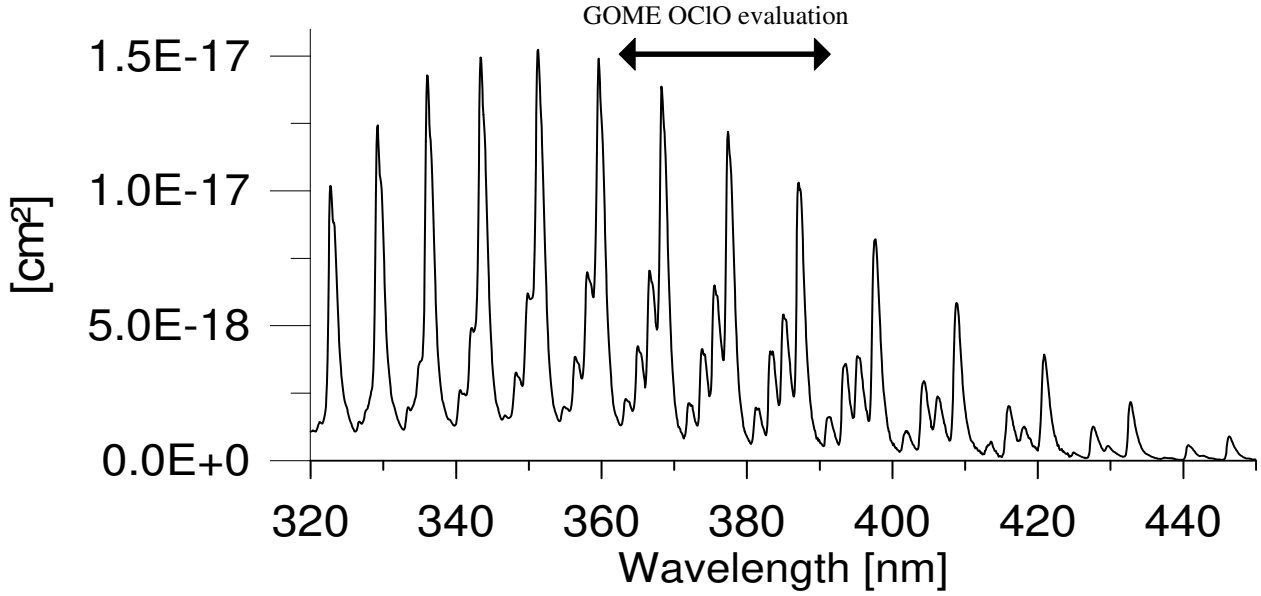

Figure 4.18 OClO cross section for 202 K [Wahner et al., 1987]. The arrows indicate the spectral range used for the OClO DOAS algorithm in this work.

For the OClO analysis the spectral range from 363 to 393 nm was chosen for several reasons:
a) The strength of the OClO cross section in that spectral region is large compared to longer wavelengths.
b) In the GOME channel 2 there are expected to be less instrumental problems than for channel 3, in particular for the wavelength range where OClO is absorbing [ESA, 1996].
c) A spectral range was searched for where as much as possible OClO absorption bands could be analysed without being affected by large Fraunhofer lines (like the CA II bands around 395 nm).
d) Below about 360 nm spectral interferences between the absorptions of OClO and O_3 might affect the OClO evaluation.
It turned out that with respect to the above considerations the wavelength range from 363 to 393 nm was best suited for the GOME OClO analysis (see Figures 4.19 and 4.20). The reference spectra used are summarised in Table 4.3. Like for the BrO analysis their relative spectral calibration with respect to the Fraunhofer spectrum was fixed and the shift of most of them is linked to the shift of the Fraunhofer spectrum during the non linear fitting process (for O_4 the spectral shift is free; see below). It turned out that the OClO absorption features in GOME spectra did not perfectly match the OClO cross section given by Wahner et al. [1987]. Using GOME spectra with large OClO absorptions, it was possible to align the OClO cross section to the atmospheric absorptions and it became obvious that the cross section must be squeezed to better match the atmospheric observations. Therefore, the wavelength calibration of the OClO cross sections used in the fitting process was slightly modified with respect to the original spectrum from Wahner et al. [1987] (see Figure 4.21).

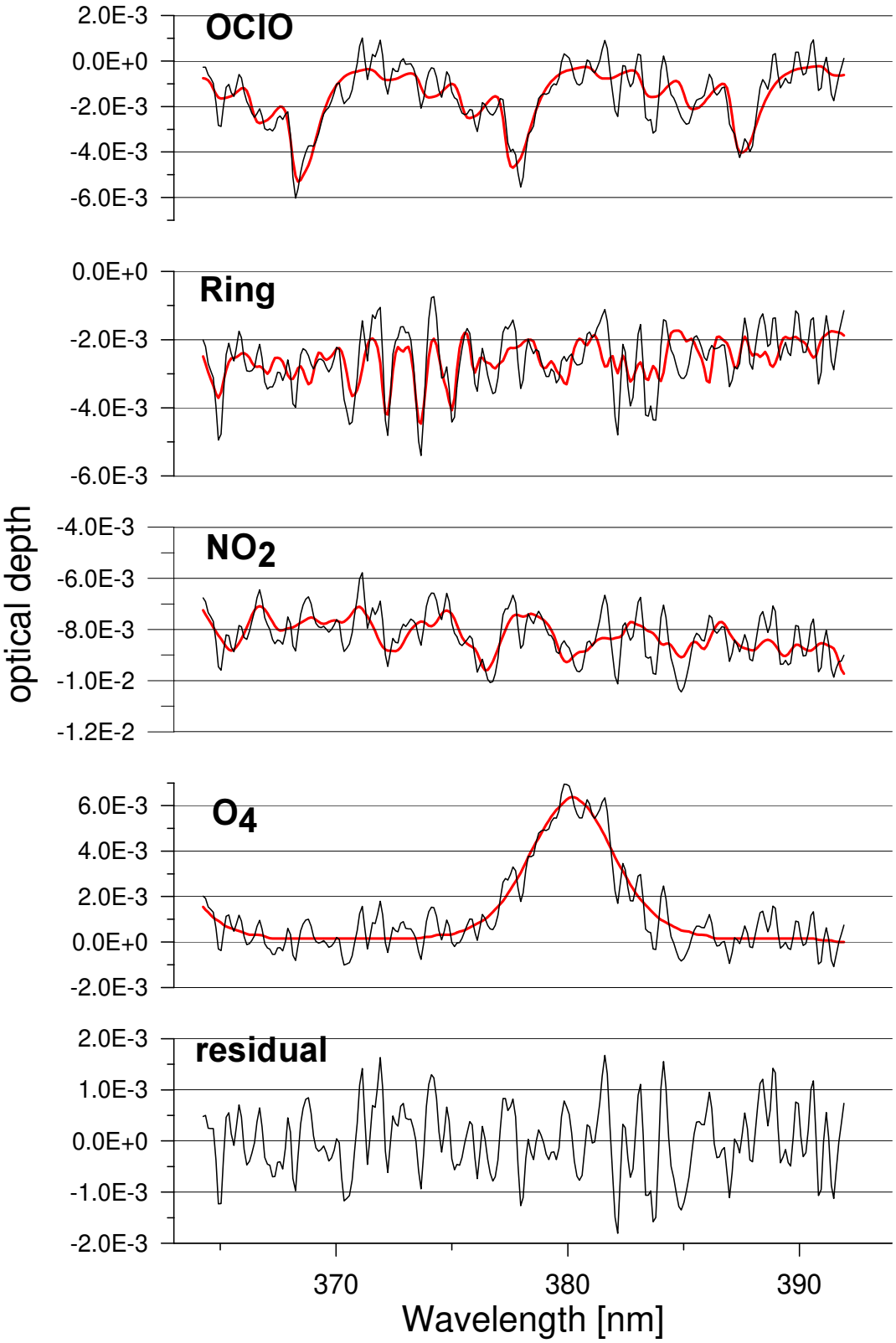

Figure 4.19 Example for the OClO evaluation of an atmospheric GOME spectrum (orbit 60918082, ground pixel # 2180, Lat.: 89.2°S, Long.: 313°E). The thick lines indicate the trace gas cross sections scaled to the respective absorptions 'found' in the GOME spectrum (thin lines).

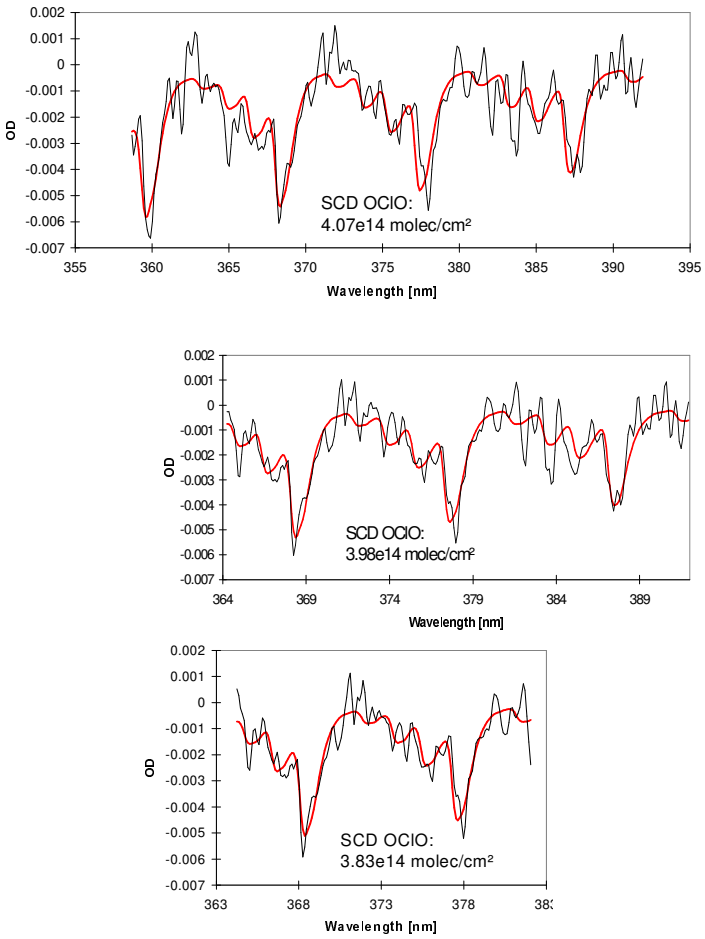

Figure 4.20 Examples for the spectral fitting of the OClO absorption in an atmospheric GOME spectrum (the same as in Figure 4.19) using different wavelength ranges. The thick lines indicate the OClO absorption spectrum scaled to the absorption found in the GOME spectrum (thin line). It can be seen that the derived OClO SCD depends slightly on the selected wavelength range. The OClO results of this PhD thesis were analysed using the wavelength range from 364 to 393 nm including 3 OClO absorption bands.

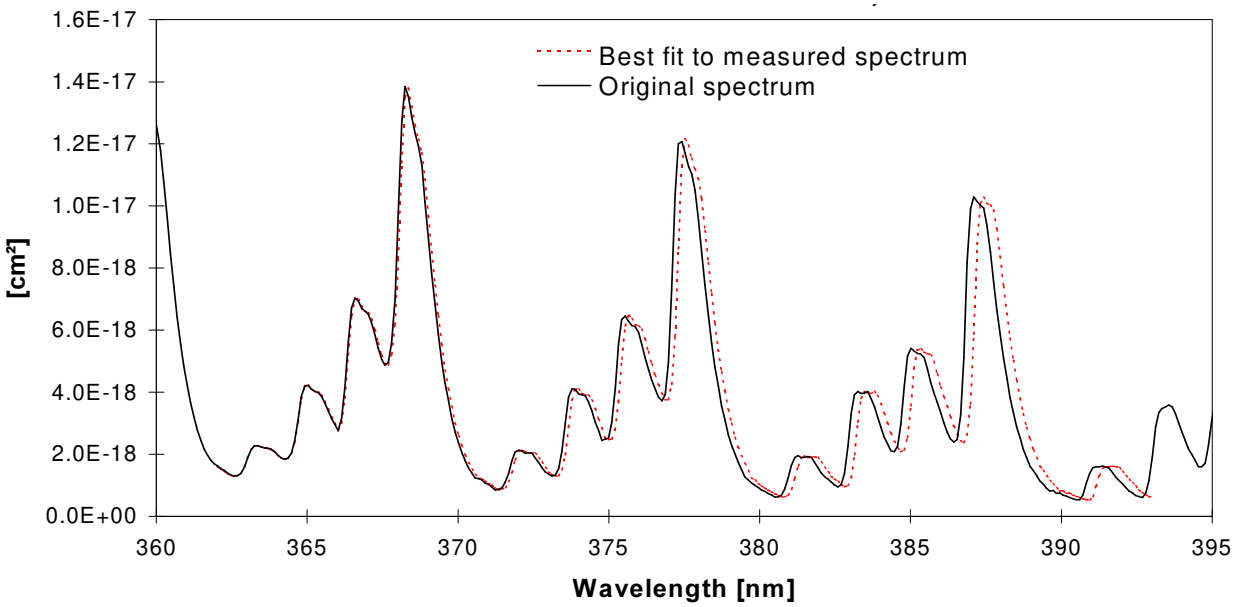

Figure 4.21 Modified wavelength calibration of the Wahner et al. [1987] cross section compared to the original one. The new cross section was determined from the best fit of the squeezed original cross section to atmospheric OClO absorptions measured in GOME spectra.

Some parameters chosen for the GOME OClO analysis are peculiar and should be described in more detail:
a) Possible spectral interference between the OClO and O_4 absorption. Although the width of both absorptions is rather different a possible spectral interference between OClO and O_4 might be caused by slight changes of the apparent O_4 absorption for scattered light measurements under different atmospheric conditions. Indications were found for such changes causing residual structures which are much narrower than the O_4 absorption itself. In particular it was found that the results of the OClO analysis showed less scatter and better agreement with the values expected from the photochemistry if the O_4 reference was allowed to shift relative to the other cross sections. For example the OClO SCDs measured for small SZA outside the polar vortex were found to be closer to zero if the shift of the O_4 reference was not linked to the shift of the Fraunhofer spectrum.
b) Although O_3 shows some weak differential absorption features in the selected spectral range it turned out that the results of the OClO analysis hardly depended on the inclusion of a O_3 cross section. In order to minimise the free parameters of the fitting procedure no O_3 cross section was included into the OClO analysis.
c) It was found that for some days the results of the OClO analysis strongly depended on the selected direct sun measurement which was used as Fraunhofer spectrum (see Figure 4.22). While the reason for this dependence is still not totally clear (it might be a result of an insufficient correction of a rapidly changing etalon structure on those days), it is obvious that the magnitude of this effect on the OClO SCDs is nearly as strong as the OClO SCDs itself. A solution was found by using a sum of 10 earth shine spectra around SZA = 70° of the same GOME orbit. Thus the time difference between the OClO measurements (made at large SZA) and the Fraunhofer spectrum is only about a few minutes. During this short time period, the changes of the instrumental properties can be expected to be negligible. Due to the small solar zenith angle of the Fraunhofer spectrum the atmospheric absorption path is short and the stratospheric OClO abundance is small because of photodissociation of the OClO molecule. In addition the location of these measurements is at lower latitudes, outside the polar vortex, and no enhanced OClO concentrations are expected even during twilight. However, if an earth shine measurement is used for the Fraunhofer spectrum instead of an observation of direct sun light it can not be ruled out that the retrieved OClO SCDs are affected by a (very small) OClO absorption in the Fraunhofer spectrum.

Reference spectrum	temperature	Source
NO_2	227 K	GOME [Burrows et al., 1998]
OClO	203 K	Wahner et al. [1987]
O_4	296 K	Greenblatt et al. [1991]
Calculated Ring spectrum	250 K	MFC, Bussemer [1993]
Fraunhofer spectrum	-	Sum of 10 GOME earth shine spectra around SZA = 70°.

Table 4.1 Reference spectra used for the GOME OClO analysis.

To account for broad band effects like Rayleigh and Mie-scattering a polynomial of degree two was also considered in the fitting process. The measured spectra and the cross sections are smoothed by convoluting with a Gaussian function with a FWHM of about 2.5 pixel. It was shown that the uncertainties of the OClO results could be significantly minimised (by up to 30%) including two Ring spectra (calculated by the approach discussed in section 4.3.4.3) instead of

one. However, the GOME OClO results presented in this PhD thesis were derived using the 'old' algorithm where only one Ring spectrum is used for the following two reasons: First, fortunately it turned out that while the uncertainties calculated by the fitting procedure were reduced the absolute values of the OClO SCDs were nearly not affected (the differences were found to be < 5%). In addition, at the time when this improvement of the OClO evaluation was achieved already a large fraction of the GOME data set was processed; thus to guarantee the continuity of the data set the implementation of the second Ring spectrum was postponed.

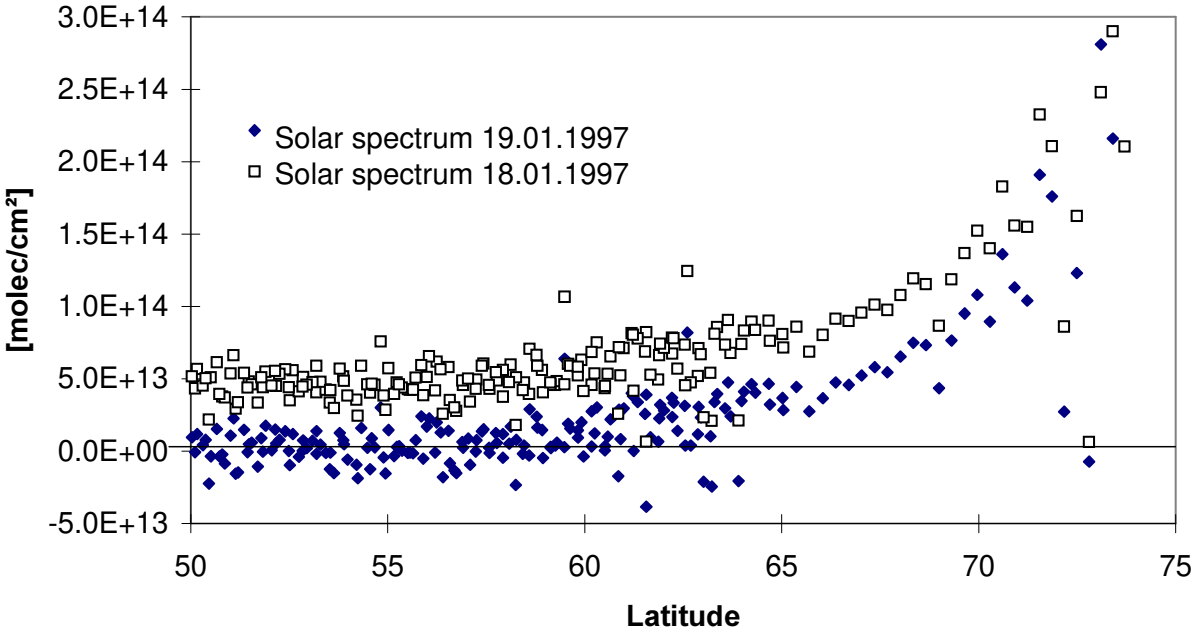

Figure 4.22 OClO SCDs retrieved for the GOME orbit 70119072, 19.01.1997 using two different solar spectra (with only one day difference) as Fraunhofer spectra. Although no OClO absorption can be expected to be present in these spectra the results of both evaluations differ strongly.

4.3.8.2 Determination of the fitting error for the GOME OClO analysis

The errors of the GOME OClO analysis were calculated as described for the BrO measurements. However, because the analysis was performed using Earth shine measurements as Fraunhofer spectra the impact of the undersampling problem is by far smaller than for the BrO evaluation and statistical errors of the linear part of the fitting process could be directly determined.
It should be noted that compared to the analysis of the BrO absorption in GOME spectra the uncertainties of the OClO analysis are quite large. This is mainly due to the small magnitude of the OClO absorption for most of the cases.
For the determination of the error of the GOME OClO analysis two measurements for different atmospheric conditions were chosen:
a) A GOME measurement for SZA = 90° for a chlorine activated stratosphere and thus with a strong OClO absorption: Ground pixel #2130 of orbit 70820222, southern hemisphere, 22.02.1997.
b) A GOME measurement for SZA = 90° but weak OClO absorption for unperturbed stratospheric conditions: Ground pixel #114 of orbit 90204150, northern hemisphere, 04.02.1999.

Since for the OClO evaluation Earth shine observations were used as Fraunhofer spectra the undersampling problem was negligible and the statistical errors could be determined straight forward from the results of the linear part of the fitting procedure [Stutz and Platt, 1996].
It was found to be about 8 % for the pixel #2130, and about 35 % for the pixel #114.
The dependence of the fitted OClO SCD on shifts in the wavelength calibration of several reference spectra used in the fitting procedure was investigated and the results are shown in Figures 4.23 a - b. It can be seen that for both ground pixel the dependence of the OClO SCD on the wavelength calibration is rather small, in particular when compared to the statistical error of the fitting process.
The uncertainty of the wavelength calibration is about ± 0.2 pixel for NO_2, and about ± 0.4 pixel for OClO, and O_4. The single errors caused by the uncertainties in the different cross section are added square. The resulting error due to the uncertainty in the wavelength calibration was found to be about 6 % for the pixel #2130, and about 10% for the pixel #114.
It should be noted that the uncertainty in the OClO cross section given by Wahner et al. [1988] of about 8% has to be taken into account when absolute OClO measurements made by GOME (or other DOAS measurements) are compared to OClO data from other observations. However, this systematic error is smaller than the errors of the fitting process. It in particular can be neglected if a relative comparison of GOME OClO measurements with other spectroscopic measurements is performed (see section 7.1.2).
The results of the error analysis for the GOME OClO analysis are summarised in Table 4.4.

Ground pixel	properties	error of the linear part of the fitting process	error due to uncertainties of the wavelength calibration	resulting error (error of cross section not included)
#2130, orbit 70820222 SZA: 90°	strong chlorine activation, SCD OClO: $2.1*10^{14}$	8 %	6 %	10 %
#114, orbit 90204150 SZA: 90°	weak chlorine activation, SCD OClO: $0.5*10^{14}$	35 %	10 %	37 %

Table 4.4 Errors of the OClO analysis of GOME spectra for different conditions of the measurements. The error of the cross section is not included, see text.

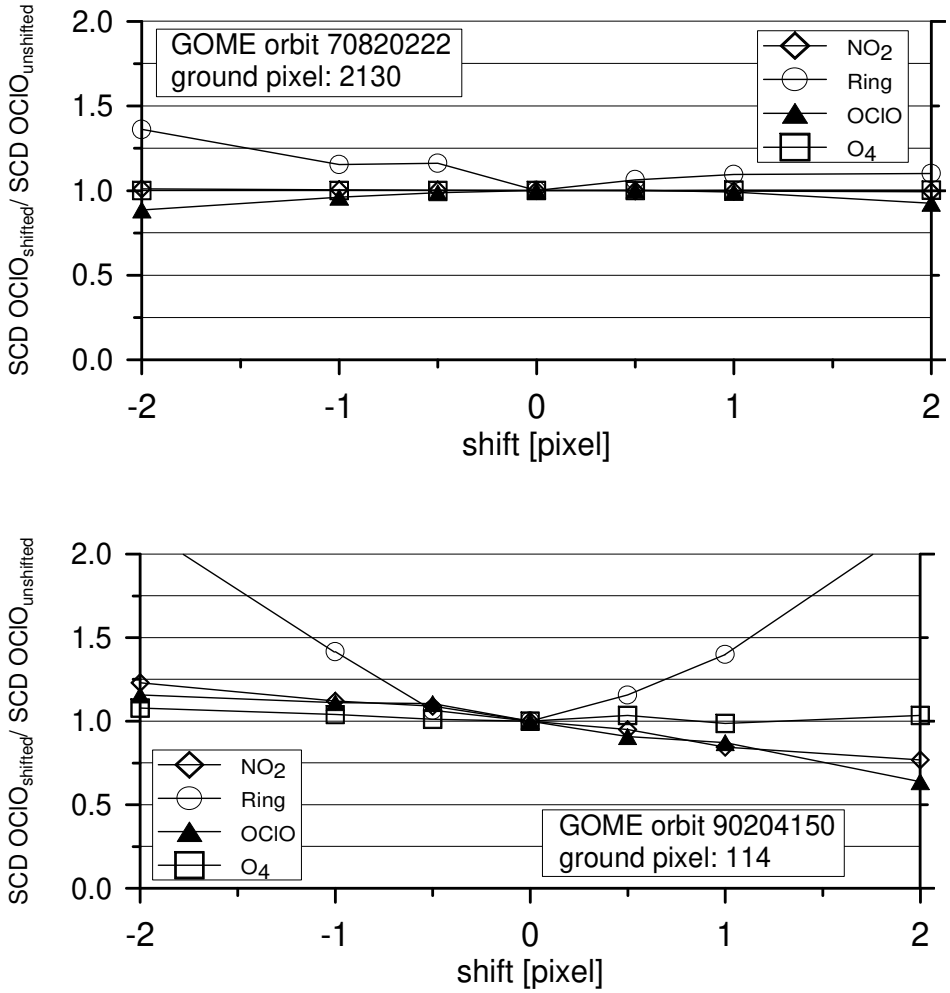

Fig. 4.23 Dependence of the OClO SCD on shifts in the wavelength calibration of the reference spectra used in the fitting procedure for the two selected GOME ground pixels.

4.3.9 Development of GOME DOAS algorithms O_3, NO_2, O_2 and O_4

Within this PhD thesis also algorithms for the retrieval of O_3, NO_2, O_2 and O_4 from GOME spectra were developed. The results of these algorithms are not the main subject of this work, but will be used in some sections, e.g. for the detection of clouds from GOME O_4 observations.
In contrast to atmospheric BrO and OClO the absorptions of these species are much stronger (up to several 10 per cents for O_2). Thus their detection in GOME spectra in general is much less dependent on the parameters of the spectral analysis.
In the following section we give a brief description of these parameters and show examples of the spectral fitting procedures.

4.3.9.1 O_3 analysis

The O_3 absorptions in the Chappuis bands were analysed in GOME spectra using a spectral range from 500 to 578 nm (see Figure 4.24). The measured spectra and the cross sections are smoothed by convoluting with a Gaussian function with a FWHM of about 2.5 pixel. Included in the fitting procedure are the reference spectra listed in Table 4.5 and a polynomial of degree 4.

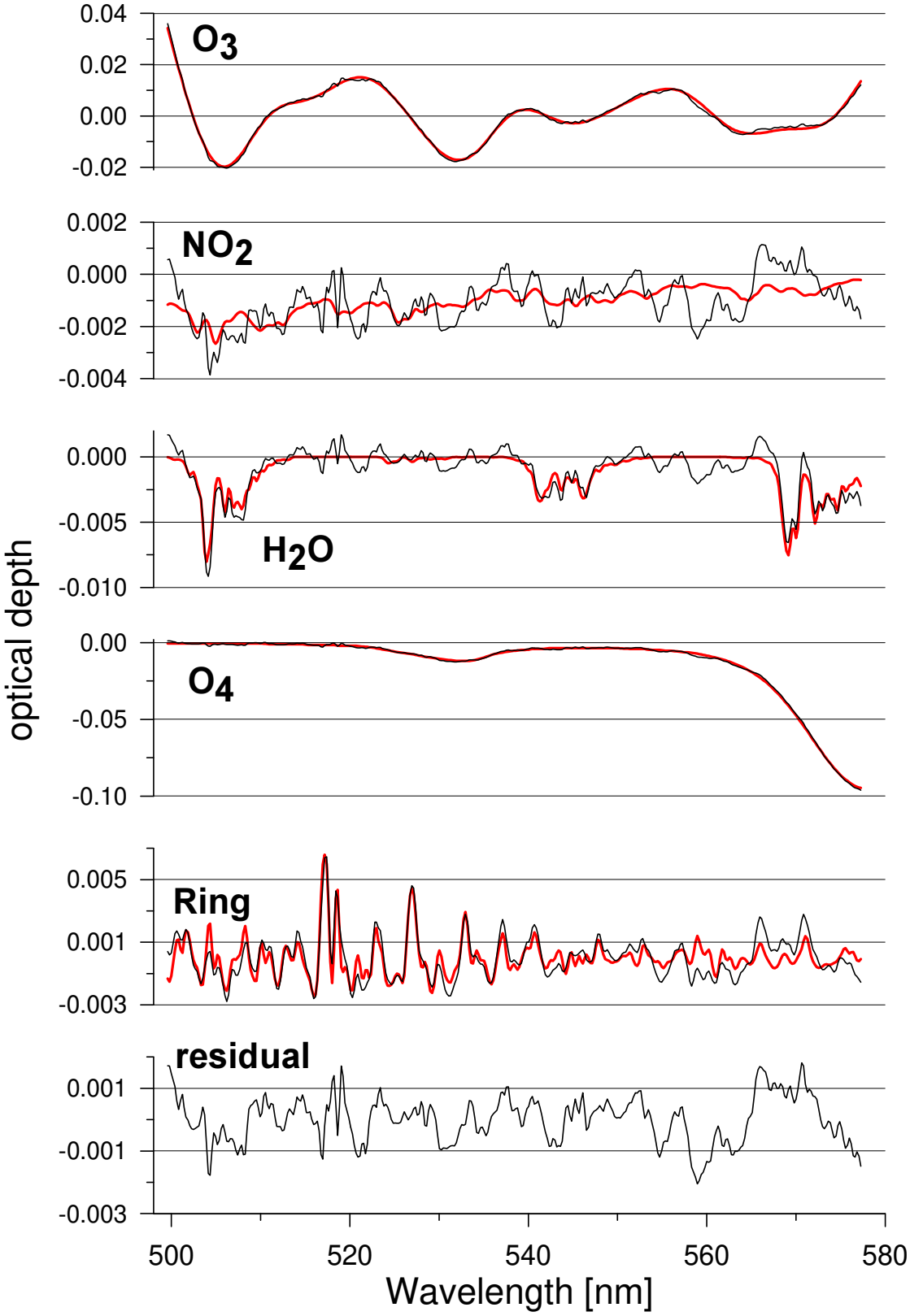

Figure 4.24 Example for the O_3 evaluation of an atmospheric GOME spectrum (GOME orbit 80206215, 21:54:19, SZA: 83.3°). The thick lines indicate the trace gas absorption spectra scaled to the respective absorptions retrieved from the GOME spectrum (thin lines).

Reference spectrum	temperature	Source
O_3	248 K	GOME [Burrows et al., 1999]
NO_2	241 K	GOME [Burrows et al., 1998]
H_2O	293 K	Rothman et al. [1992]
O_4	296 K	Greenblatt et al. [1991]
Calculated Ring spectrum	250 K	MFC, Bussemer [1993]
Fraunhofer spectrum	-	GOME direct sun light

Table 4.5 Reference spectra used for the GOME O_3 analysis.

4.3.9.2 NO_2 analysis

The NO_2 absorptions were analysed in GOME spectra using a spectral range from 431 to 452 nm (see Figure 4.25). The measured spectra and the cross sections are smoothed by convoluting with a Gaussian function with a FWHM of about 2.5 pixel. Included in the fitting procedure are the reference spectra listed in Table 4.6 and a polynomial of degree 2.

Reference spectrum	temperature	Source
O_3	221 K	GOME [Burrows et al., 1999]
NO_2	221 K	GOME [Burrows et al., 1998]
H_2O	293 K	Rothman et al. [1992]
Calculated Ring spectrum	250 K	MFC, Bussemer [1993]
Fraunhofer spectrum	-	GOME direct sun light

Table 4.6 Reference spectra used for the GOME NO_2 analysis.

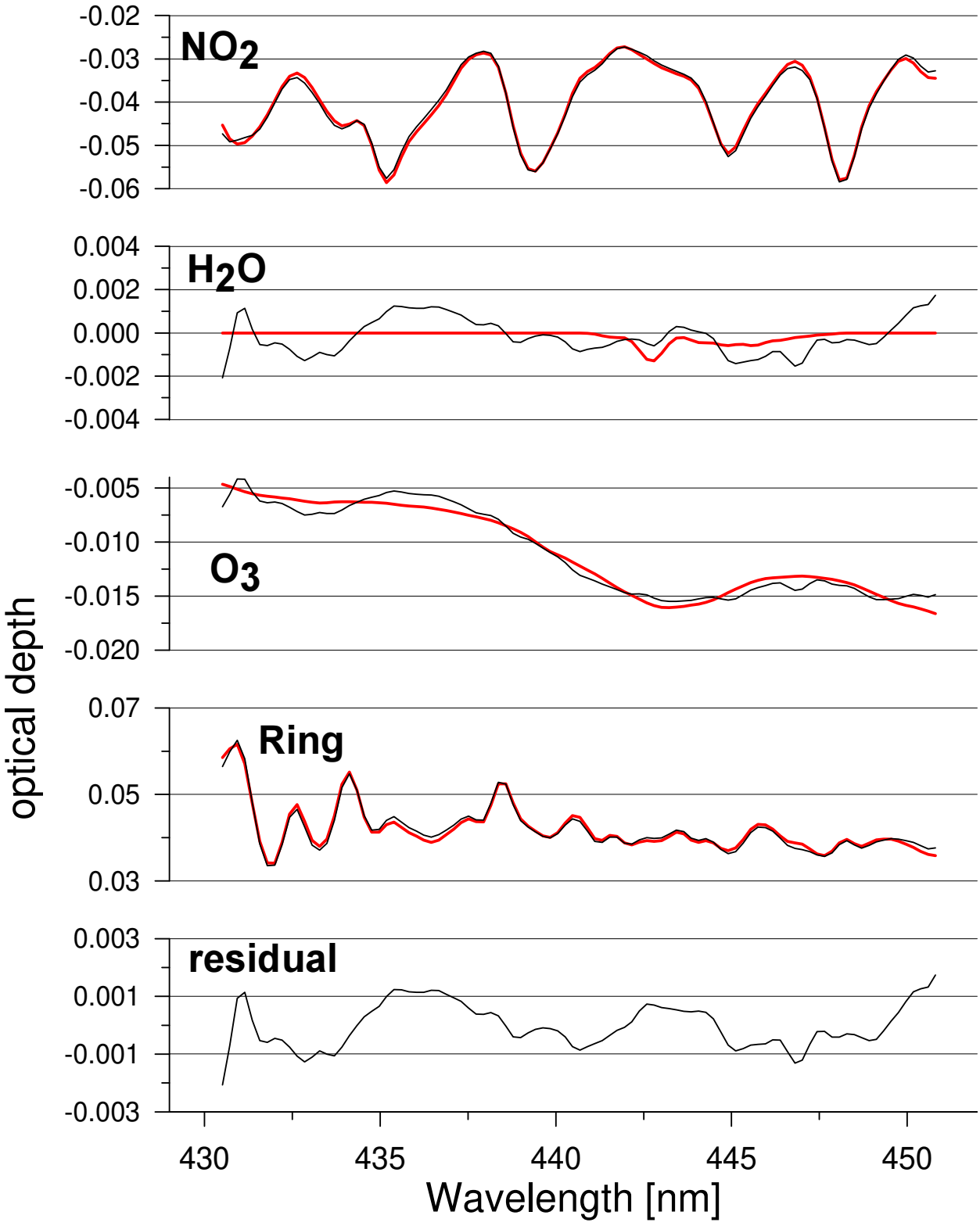

Figure 4.26 Example for the O_3 evaluation of an atmospheric GOME spectrum (GOME orbit 71127003, 01:27:50, SZA: 88.9°). The thick lines indicate the trace gas absorption spectra scaled to the respective absorptions retrieved from the GOME spectrum (thin lines).

4.3.9.2 O_2 and O_4 analysis

The O_2- and O_4-absorptions were analysed in GOME spectra using a spectral range from 599 to 645 nm (see Figure 4.26). The measured spectra and the cross sections are smoothed by convoluting with a Gaussian function with a FWHM of about 2.5 pixel. Included in the fitting procedure are the reference spectra listed in Table 4.7 and a polynomial of degree 2.

Reference spectrum	temperature	Source
O_2	293 K	Rothman et al. [1992]
O_4	296 K	Greenblatt et al. [1991]
H_2O	293 K	Rothman et al. [1992]
Calculated Ring spectrum	250 K	MFC, Bussemer [1993]
Fraunhofer spectrum	-	GOME direct sun light

Table 4.7 Reference spectra used for the GOME O_2- and O_4 analysis.

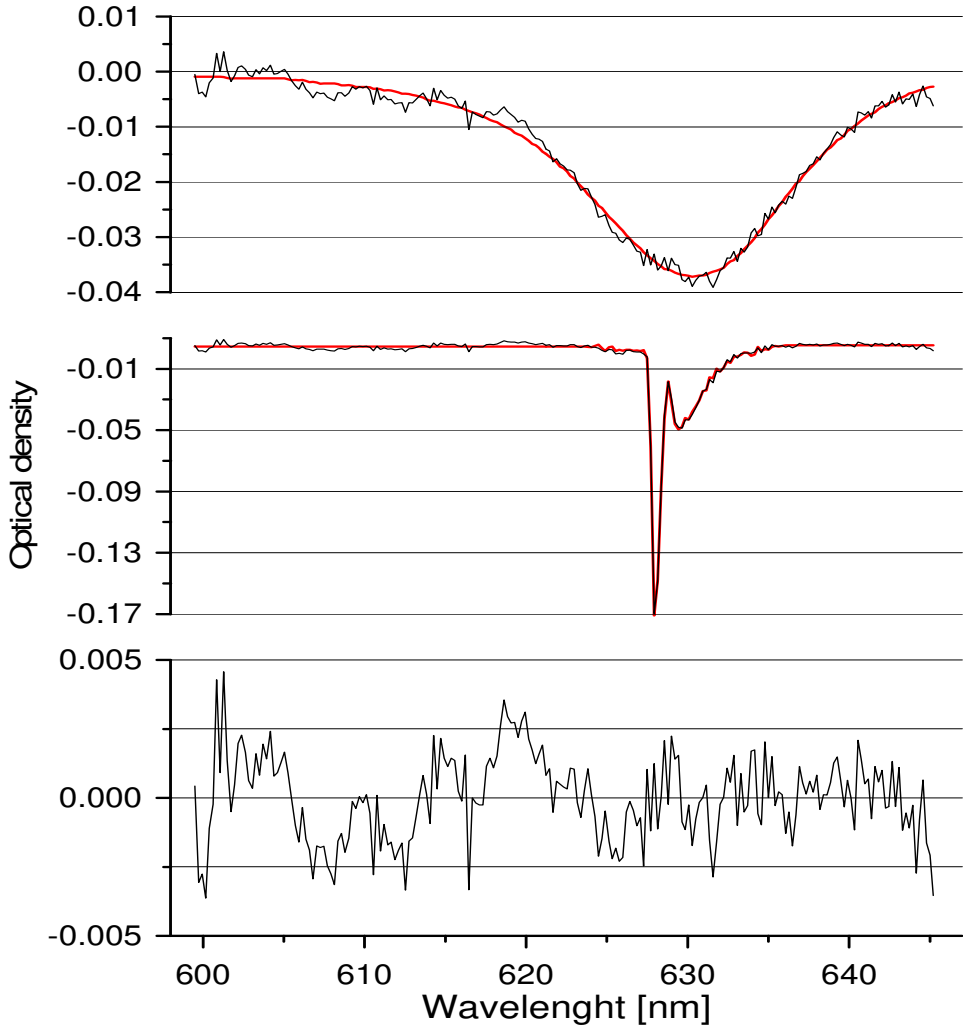

Figure 4.27 Example for the analysis of O_2 and O_4 in atmospheric GOME spectrum (GOME orbit 60701125, 11:29:53, SZA: 67.5°). The thick lines indicate the trace gas absorption spectra scaled to the respective absorptions retrieved from the GOME spectrum (thin lines).